The unexplored functions of Toll-like receptor signaling: immunometabolism, development and microbiome interactions

Liu, L.

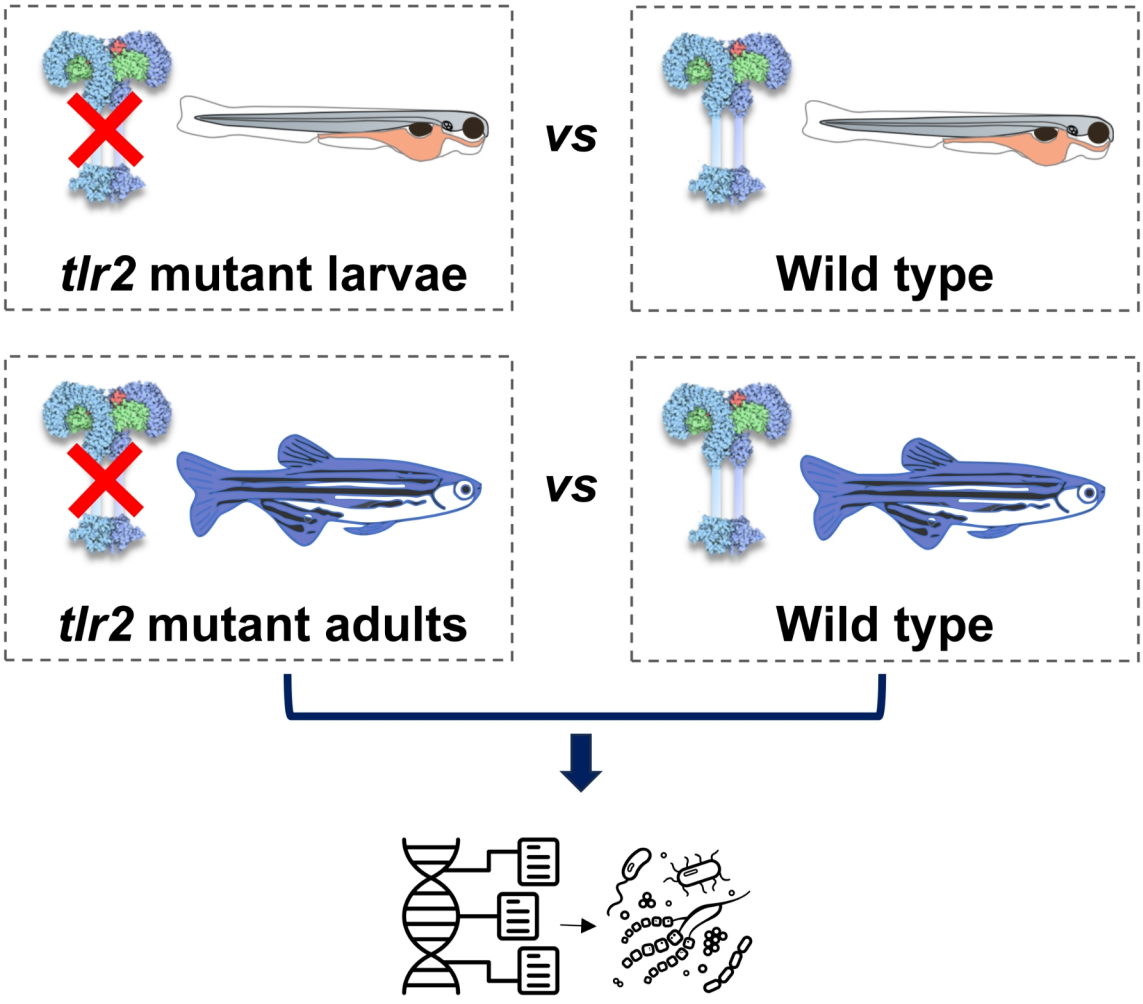
vs
tlr2 mutant larvae
Wild type
vs
tlr2 mutant adults
Wild type
Microbiome profiling

Chapter 4

The function of Toll-like receptor 2 in control of transcriptome responses to the microbiome and microbiome composition

Li Liu and Herman P. Spaink*

Institute of Biology Leiden, Animal Science and Health, Leiden University, Einsteinweg 55, 2333 CC Leiden, The Netherlands

* Correspondence: h.p.spaink@biology.leidenuniv.nl (H.P.S.)

Published in ***Animal Microbiome*** 2026; 8(1):5. doi: 10.1186/s42523-025-00502-z

Abstract

Background: Toll-like receptor 2 (TLR2) plays a pivotal role in innate immunity and has recently emerged as a critical regulator of host-microbiome interactions. However, how TLR2 influences host transcriptional responses to colonized microbiome and microbial community dynamics remains largely unclear. A comparison between germ free (GF) and conventionalized zebrafish (*Danio rerio*) larvae provides a valuable system to investigate how the microbiome influences host transcriptomic responses in a *tlr2* mutant versus wild-type control. *Vice versa*, to understand the role of Tlr2 in regulating the microbiome, we have analyzed microbial community composition in both *tlr2* mutant and wild-type zebrafish at larval and adult stages.

Results: RNAseq analysis revealed that approximately 2.6% of the zebrafish genome (827 genes) exhibited transcriptomic alterations in *tlr2* mutant larvae compared to the wild type under microbiome-colonized conditions, whereas around 2% of the genome (639 genes) showed differential expression under GF conditions. KEGG enrichment analyses show that under both microbiome-colonized and GF conditions major differences between the *tlr2* mutant and wild type are related to metabolism. Furthermore, there is a striking difference in endoplasmic reticulum stress responses, including well-known markers for inflammatory bowel disease which are all downregulated in the mutant under the microbiome-colonized condition. Microbiome colonization elicited a broader transcriptional response in wild-type larvae than in the mutant, with specifically the ferroptosis and apoptosis and inflammation related pathways differently regulated. In terms of how Tlr2 influences microbial composition, 16S rRNA gene sequencing showed large differences in beta diversity between the *tlr2* mutant and wild type. The *tlr2* mutant exhibited higher microbial alpha diversity during early development, whereas alpha diversity was higher in wild-type adults. For larvae at the genus level, *tlr2* mutant larvae showed increased *Chryseobacterium* and *Flectobacillus* but reduced *Gracilibacteria* abundance relative to wild-type controls. For adult gut samples, the relative abundance of *Cetobacterium* was higher in the *tlr2* mutants, indicating a developmental stage-specific restructuring of the microbiome.

Conclusions: TLR2 not only modulates host transcriptional responses to microbial colonization, but also shapes gut microbial diversity, composition, and metabolic potential. Our findings highlight the critical role of TLR2 in orchestrating immune-metabolic

homeostasis and provide new insights into its broader function in maintaining host-microbiota symbiosis across developmental stages.

Keywords: TLR2; zebrafish; microbiome composition; microbial diversity

1. Introduction

Toll-like receptors (TLRs) are a family of pattern recognition receptors (PRRs) that play a central role in the innate immune system by detecting pathogen-associated molecular patterns (PAMPs) derived from invading pathogens and host-derived damage-associated molecular patterns (DAMPs) released from damaged cells [1, 2]. Among them, Toll-like receptor 2 (TLR2) is particularly notable for its ability to recognize a broad spectrum of microbial components, including bacterial lipoproteins, glycolipids and peptidoglycans, through heterodimerization with TLR1 or TLR6 [3-5]. Upon ligand recognition, TLR2 activates downstream signaling cascades involving adaptor proteins such as Myeloid differentiation factor 88 (MyD88), leading innate immune cells to produce inflammatory cytokines and antimicrobial responses [6-8].

Nowadays, beyond its classical immune functions in pathogen recognition, TLR2 has emerged as a key regulator of host-microbiota interactions, metabolic homeostasis, mucosal immunity and secretion of antimicrobial compounds in the gut [9-12]. Owing to these functions, TLR2 is assumed to control microbial colonization in the gut and determine diversity of the microbiome, i.e. the complete collection of the microorganisms [13, 14]. Underscoring this assumption, it has been shown that TLR2 not only detects microbial-associated molecular patterns in the gut but also actively modulates the composition and functional dynamics of the gut microbiota [15]. By regulating host immune response to commensal and opportunistic microbes, TLR2 contributes to maintaining gut homeostasis by balancing tolerance and vigilance [15, 16]. Disruption of TLR2 signaling has been closely linked to microbial dysbiosis as a result of antibiotic treatments and increased susceptibility to infection, showing its essential role in maintaining host-microbe homeostasis [17]. For example, impaired TLR2 activation resulting from such severe gut dysbiosis has been implicated in increased vulnerability to nontuberculous mycobacterial infections [17]. It has also been shown that TLR2 is involved in maintaining metabolic homeostasis in the absence of infection [18]. These observations suggest that functional TLR2 signaling is vital for

preventing pathological dysbiosis and maintaining host homeostasis and effective immune defense.

Among the microbial habitats in a host, the gut microbiome is the most densely populated and extensively studied. Increasing evidence suggests that microbiome especially gut microbiota plays a critical role in host homeostasis, large discrepancies of the microbiome has been closely associated with a range of metabolic and inflammatory disorders, including obesity, inflammatory bowel disease (IBD) and colorectal cancer (CRC) [12, 16]. The components of the gut microbiota interact with specific TLRs such as TLR2 to contribute to whole-body immune and metabolic homeostasis via mechanisms that are still poorly understood [12].Therefore, understanding the complex interplay between TLR2 and the microbiome not only reveals fundamental insights into mucosal immunity, but also provides potential therapeutic strategies in dysbiosis-related diseases such as IBD and CRC.

Zebrafish (*Danio rerio*) have become an established model for studying host-microbiota interactions due to their genetic tractability and amenability to versatile gnotobiotic techniques [19, 20]. The zebrafish gut shares many anatomical and physiological features with the human gastrointestinal tract, including epithelial cell types, mucus production, innate immune components, and functional regionalization [21, 22]. Additionally, the zebrafish microbiome exhibits taxonomic and functional similarities to that of mammals, making it a relevant system for translational microbiome research [21, 22]. Importantly, zebrafish larvae can be raised germ free and subsequently colonized with defined microbial communities, providing a powerful platform to study host transcriptomic responses to colonized microbiome.

In this study, we aimed to investigate the role of TLR2 in regulating transcriptomic responses to microbiota colonization and shaping gut microbial composition. We generated *tlr2* mutant zebrafish and wild-type controls and employed germ free and conventionalized zebrafish models. Using zebrafish larval model, we first performed RNAseq for germ free and microbiome colonized larvae for both genotypes (*tlr2* wild type and mutant) to study host transcriptomic responses. Using both larval and adult zebrafish as a model, we did 16S rRNA gene amplicon sequencing on *tlr2* wild-type and mutant zebrafish to detect the microbial diversity, composition, and metabolic potential across developmental stages. Our findings provide new insights into the function of TLR2 in coordinating host-microbiome crosstalk.

2. Materials and Methods

2.1. Zebrafish maintenance and mutant line construction

All adult and larval zebrafish used in this study were maintained at Leiden University in accordance with the standard protocols (zfin.org) and adhered to the international guidelines specified by the EU Animal Protection Directive 2010/63/EU. The culture of adult fish was approved by the university's local animal welfare committee (DEC) (License number: protocol 14,198). Adult fish were kept at 28°C on a 14 h:10 h light-dark cycle and maintained in a recirculating aquaculture system according to standard protocols (zfin.org). Adults were fed twice daily with a combination of dry flake food (Tetramin, Tetra, Germany) and live *Artemia* nauplii. Eggs and larvae were grown in laboratory-manufactured egg water (containing 60 mg/l instant ocean sea salts) at 28.5°C. For RNAseq and 16S rRNA gene sequencing of larvae, the experiments were performed on larvae at 5 days post fertilization (dpf). For 16S rRNA gene sequencing of gut adult samples, one-year-old fish were euthanized in the morning prior to feeding to minimize circadian and feeding-related variation, following standard protocols (zfin.org).

The *tlr2*^{sa19423} mutant (further referred as *tlr2*$^{-/-}$ or *tlr2* mutant) line was identified by the sequencing of an ENU-mutagenized zebrafish library (ZFIN Cat# ZDB-ALT-131217–14694, RRID: ZFIN_ZDB-ALT-131217–14694) [23]. All mutant alleles were identified by sequencing and the homozygote carriers of the mutations were outcrossed more than three times to wild type (AB/TL strains). Homozygote mutants and their wild type siblings (further referred as *tlr2*$^{+/+}$) were used to generate models in this study.

2.2. Germ free larvae generation

Germ free (GF) and conventionalized (CONVD) embryo groups were generated according to the previously described "Natural breeding method" with several modifications [24, 25]. Briefly, all collected embryos were divided into two groups. One group was treated with an antibiotic mix consisting of Ampicillin (250 µg/ml), Kanamycin (5 µg/ml) and amphotericin B (250 ng/ml), and maintained in autoclaved sterile egg water (60 mg/l instant ocean sea salts). At 6 hours post fertilization (hpf), all embryos from this group were washed using 0.2 % PVP-I and 0.003% bleach to process the sterilization. Another group was maintained in a non-sterile egg water without any treatment and served as the conventionally reared control.

At 2.5 dpf, half of the sterilized larvae were randomly selected and exposed to the microbial environment by transferring them into water collected from the petri dishes containing conventionally reared larvae, thereby generating the CONVD group. The remaining sterilized larvae were kept in sterile egg water as the GF group. Only morphologically normal larvae were included in subsequent analyses. Sterile conditions in GF groups were monitored by incubating 2 ml water from the GF group petri dish on Luria-Bertani (LB) agar plates under aerobic conditions at 28 °C for 2 days.

2.3. RNAseq processing and analysis

For the purpose of RNA sequencing, the extraction of total RNA from 5 dpf *tlr2* mutant zebrafish larvae and wild type controls in both CONVD and GF conditions was performed using TRIzol Reagent (Life Technologies), following the manufacturer's instructions. For each group, three biological replicates were prepared, with 100 larvae pooled per replicate. DNase treatment was then conducted by using the kit (Thermo Scientific) to remove the DNA contamination. RNA sequencing of larvae from four experimental groups (GF *tlr2* wild-type group, GF *tlr2* mutant group, CONVD *tlr2* wild-type group and CONVD *tlr2* mutant group) was conducted by GenomeScan B.V. (Leiden, The Netherlands) as previously described [23]. Sequencing data of three biological replicates for the four experimental groups were aligned and mapped to the zebrafish genome GRCz11 using Salmon v1.2.1 [26]. Differentially expressed genes (DEGs) were analyzed using DESeq2 v1.24.0 [27]. Gene expression differences between experimental groups were tested using the Wald test implemented in DESeq2. P-values were adjusted for multiple testing using the Benjamini–Hochberg false discovery rate (FDR) correction, and statistical significance was determined by an adjusted p-value (padi value) less than 0.05 [28]. KEGG (Kyoto Encyclopedia of Genes and Genomes) pathway enrichment analysis was performed in DAVID Bioinformatics Resources 6.8 (https://david.Ncifcrf.Gov/).

2.4. qRT-PCR validation

After the extraction of total RNA, we left some RNA for the cDNA synthesis and then performed qRT-PCR validations. The qRT-PCR validation was performed on a CFX96TM Touch Real-Time PCR Detection (Bio-Rad Laboratories, Inc, USA) to detect the expression profiles of DEGs in representative enrichment pathways. The peptidylprolyl isomerase A-like

(*ppial*) gene was used to be the reference gene. The sequences of primers used in this study were showed in Supplementary Table 1. The qRT-PCR reaction procedure was performed according to the following protocol: 95℃ 3 min, 40 cycles real time of 95℃ 15 sec, 68℃ 30 sec and 72℃ 30 sec, and final melting curve of 95℃ 1 min and 55℃ 10 sec. The quantitative qRT-PCR assay was biologically repeated for three times and the relative expression level was determined by the comparative $2^{-\Delta\Delta Ct}$ method [29].

2.5. Sample collection, DNA preparation and 16S rRNA gene sequencing

For the purpose of 16S rRNA gene sequencing of *tlr2* wild-type and mutant larvae, 20 larvae at 5 dpf as a pool, 4 pools for each genotype were collected to extract DNA using a kit following manufacturer instructions. For the 16S rRNA gene sequencing of gut samples from adult *tlr2* wild-type and mutant zebrafish, 10 fish from each genotype were euthanized and their entire guts were aseptically extracted and collected under sterile condition for DNA extraction. A total of 30 ng qualified DNA template and the 16S rRNA fusion primers (targeting the V3-V4 region, the sequences of primers were shown in Supplementary Table 1) were added for PCR amplification. PCR products are purified using Agencourt AMPure XP beads, dissolved in Elution Buffer and subsequently labeled to complete library construction. Library size and concentration were detected by Agilent 2100 Bioanalyzer. Qualified libraries are sequenced on the DNA Nanoball (DNB) sequencing platform with sequencing parameters selected based on the insert size.

2.6. Bioinformatic analysis for 16S rRNA gene sequencing

Raw data were filtered to generate high quality clean reads using iTools Fqtools fqcheck (v.0.25) developed by BGI Genomics (Shenzhen, China) and Cutadapt (v2.6) as follows: 1) Truncate reads whose average Phred quality values were lower than 20 over a 25 bp sliding window would be truncated. Remove reads whose length were lower than 75% of their original lengths after truncation; 2) Remove reads that were contaminated by adapter sequences (default parameter:15 bases overlapped by reads and adapter with maximal 3 bases mismatch allowed); 3) Remove reads with ambiguous base (N base); 4) Remove low-complexity reads (default parameter: reads with 10 consecutive same base) [30]. To ensure the removal of barcode sequences from pooling libraries, clean reads were assigned to

corresponding samples through alignments (0 base mismatch) against barcode sequences by in-house scripts.

After data filtering to get clean data, reads with overlaps were stitched to generate consensus sequences using FLASH (Fast Length Adjustment of Short reads, v1.2.11) software. Next, these consensus sequences were imported into the QIIME 2 (Quantitative Insights Into Microbial Ecology, Flagstaff, AZ, USA, Version 1.9.1) and denoised using the DADA2 algorithm. Following denoising, representative sequences were further clustered into operational taxonomic units (OTUs) at 97% sequence similarity to ensure compatibility with legacy taxonomic databases using the QIIME vsearch cluster-features-de-novo method. Taxonomic classification of the OTUs was performed using a Naive Bayes classifier trained on the SILVA 138 database at 99% identity. The resulting OTU table and corresponding taxonomic annotation table were used in subsequent diversity and compositional analyses.

Alpha rarefaction analysis which enables evaluation of sequencing depth sufficiency across samples and Pielou's evenness were performed using QIIME 2. For additional diversity analyses, the MicrobiomeAnalyst web platform (https://www.microbiomeanalyst.ca) was used. Specifically, Shannon index, observed species, and Simpson index were calculated to assess alpha diversity, while Principal Coordinates Analysis (PCoA) based on Bray-Curtis dissimilarity was used to evaluate beta diversity and visualize differences in microbial community structure between groups. All diversity analyses were conducted after normalization and filtering steps as recommended by MicrobiomeAnalyst's standard pipeline [31]. For compositional analyses, OTU-based taxonomic annotations were used to quantify the number of sequences assigned to each taxonomic rank (class, family and genus for larvae, genus for adult) for each sample. The resulting counts were converted to relative abundances to enable comparison of microbial community composition across samples. Statistical comparisons of relative taxon abundances were performed using PERMANOVA test. Microbial functional prediction was then performed using PICRUSt2 (Phylogenetic Investigation of Communities by Reconstruction of Unobserved States 2) software based on 16S rRNA gene sequencing data. The OTU data obtained from QIIME2 were first placed into a reference phylogenetic tree to predict gene family abundances. The resulting functional annotations were then mapped to the MetaCyc (a metabolic pathway database) databases to classify and predict the potential pathways of microbial communities. Predicted functional pathways were categorized at level 2 of the MetaCyc hierarchies. For each pathway, relative

abundance (%), $\log_2$ fold change between groups, and *P* values and FDR-adjusted *P*-values were calculated. Statistical comparisons were performed using Wilcoxon rank-sum test.

2.7. Statistical analysis

The statistical analysis was performed using the Graphpad Prism software (Version 10; GraphPad Software, San Diego, CA, USA). All experimental data in this study are shown as mean ± the standard deviation (SD). D'Agostino-Pearson and Shapiro-Wilk normality test was performed to determine the Gaussian distribution of the data. The statistical significant differences of alpha diversity indices between groups was determined using t test. Significant differences in relative taxonomic abundances between groups was assessed using two-way analysis of variance (ANOVA) and the Tukey-Kramer method was used for post hoc analysis. The significance was established as * $P < 0.05$, ** $P < 0.01$, *** $P < 0.001$ and **** $P < 0.0001$.

3. Results

3.1. Transcriptomic alterations caused by *tlr2* mutation in the presence or absence of a microbiome

To investigate whether transcriptomic differences between *tlr2* mutant zebrafish larvae and wild type controls are influenced by the presence or absence of a microbiome, we generated both germ free (GF) and conventionalized (CONVD) larvae from *tlr2* wild-type and mutant zebrafish lines and then performed RNAseq studies (Figure 1A). In the CONVD condition, a signature set of 827 significantly differentially expressed genes (DEGs) were identified in *tlr2* mutant larvae compared to wild-type controls (padj value < 0.05), comprising 317 upregulated and 510 downregulated genes (Figure 1B). In the GF condition, a signature set of 639 DEGs were detected in the *tlr2* mutant larvae compared with the wild-type controls (padj value < 0.05), including 227 upregulated genes and 412 downregulated genes (Figure 1B). Among these, 122 upregulated and 241 downregulated DEGs were shared between the CONVD and GF conditions, indicating a core set of *tlr2*-dependent transcriptional changes that are regulated in the same way irrespective of microbiome colonization status. Moreover, the total number of DEGs was notably higher in the presence of the microbiome compared to the GF condition, suggesting that *tlr2* mutation has a more pronounced impact on host transcriptional responses when microbial signals are present.

For gene enrichment analysis of DEG signature sets identified above, KEGG pathway enrichment analysis was performed using the DAVID bioinformatics program. The raw data for the DEGs from the representative pathways in *tlr2* mutant larvae compared to wild-type controls under the CONVD condition and GF condition are shown in Supplementary table 2 and 3, respectively. In summary, in the *tlr2* mutant differential expression signature under the CONVD condition, for both upregulated and downregulated DEGs, the enriched KEGG pathways were dominated by metabolic related pathways (Figure 1C,E). In addition, downregulated DEGs under the CONVD condition enriched in the protein processing in endoplasmic reticulum pathway and apoptosis (Figure 1E). Under the GF condition, for upregulated DEGs, the significantly enriched KEGG pathways included apelin signaling pathway and glycerolipid metabolism (Figure 1D). Specifically, downregulated DEGs under the GF condition enriched in ferroptosis and p53 signaling pathways (Figure 1F). These analyses revealed both shared and microbiome condition-specific transcriptional alterations associated with *tlr2* mutation. Metabolic pathways, biosynthesis of cofactors, amino sugar and nucleotide sugar metabolism, and apoptosis were consistently enriched in both CONVD and GF conditions, indicating a core set of *tlr2*-regulated pathways independent of microbiota status. In contrast, CONVD-specific enrichment was observed in pathways related to endoplasmic reticulum stress response (e.g., protein processing in the endoplasmic reticulum) and carbohydrate metabolism (e.g., glycolysis/gluconeogenesis, carbon metabolism). Specifically, in the protein processing in endoplasmic reticulum pathway, all the DEGs were consistently downregulated in the *tlr2* mutant larvae (Figure 1E). In the glycolysis/gluconeogenesis pathway, all the DEGs that could be associated with this pathway were downregulated in the *tlr2* mutant larvae (Figure 1E). However, GF-specific enrichment included pathways such as ferroptosis and p53 signaling. For example, in the ferroptosis pathway, all associated DEGs were downregulated in *tlr2* mutant larvae (Figure 1F). In the p53 signaling pathway, all DEGs were downregulated in *tlr2* mutant larvae (Figure 1F). These results indicate distinct cellular adaptation mechanisms for *tlr2* deficiency in the presence or absence of a microbiome.

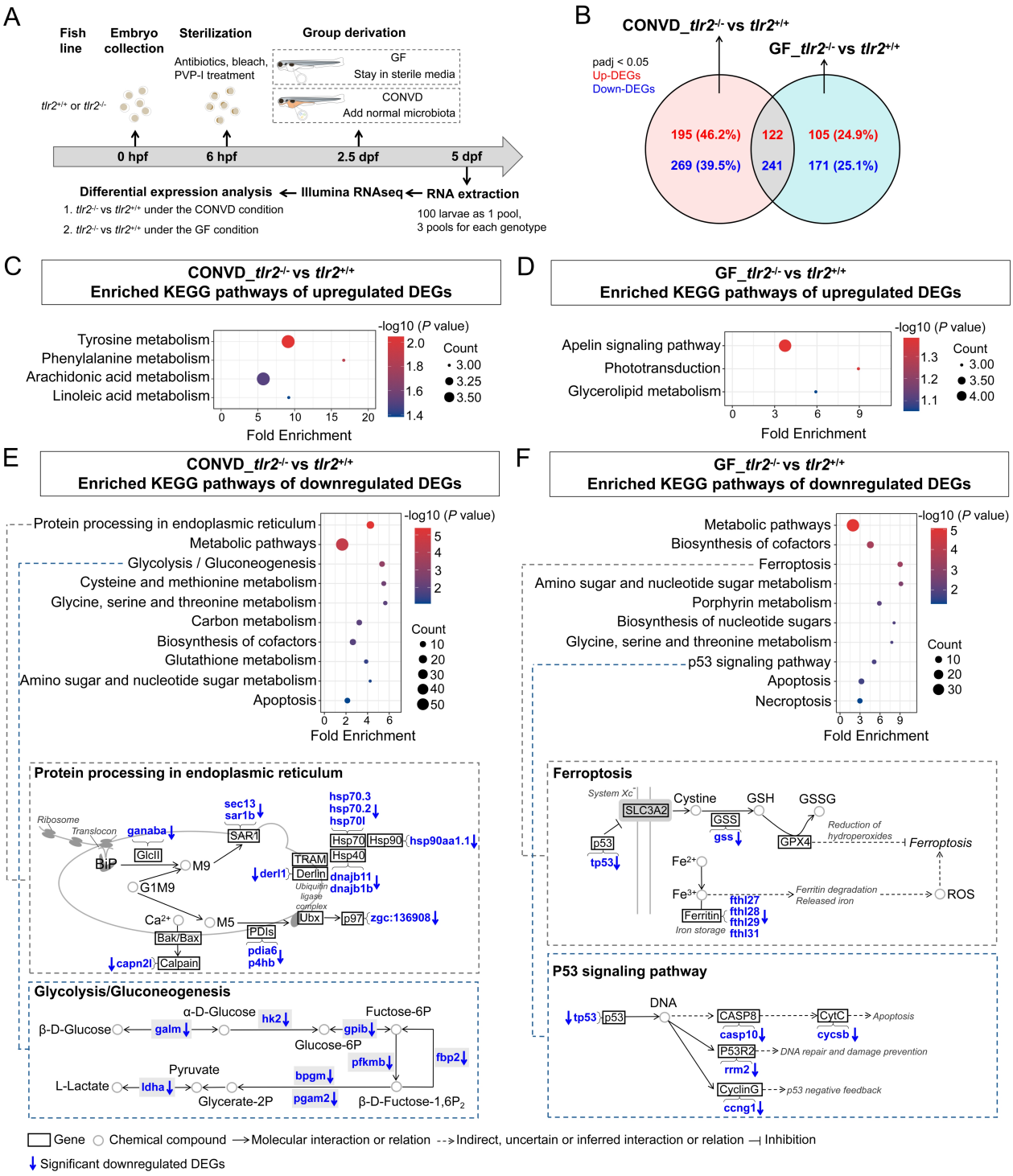

Figure 1. Differential gene expression profiles resulting from *tlr2* mutation under CONVD and GF conditions. (A) Schematic of the experimental workflow. Conventionalized (CONVD) and germ free (GF) zebrafish larvae derived from *tlr2* wild-type and mutant lines were used to performed RNAseq at 5 days post fertilization (dpf). Differential expression analysis was conducted between *tlr2*$^{-/-}$ and *tlr2*$^{+/+}$ zebrafish larvae under CONVD or GF condition. (B) Numbers of upregulated and downregulated significantly differentially expressed genes (DEGs) in *tlr2*$^{-/-}$ versus *tlr2*$^{+/+}$ zebrafish larvae under CONVD and GF conditions. DEGs were

assessed by padj value less than 0.05. (C) Enriched KEGG pathway of upregulated DEGs in *tlr2*$^{-/-}$ versus *tlr2*$^{+/+}$ zebrafish larvae under the CONVD condition. (D) Enriched KEGG pathway of upregulated DEGs in *tlr2*$^{-/-}$ versus *tlr2*$^{+/+}$ zebrafish larvae under the GF condition. (E) Enriched KEGG pathway of downregulated DEGs in *tlr2*$^{-/-}$ versus *tlr2*$^{+/+}$ zebrafish larvae under the CONVD condition and schematic diagram of DEGs in the representative pathways. (F) Enriched KEGG pathway of downregulated DEGs in *tlr2*$^{-/-}$ versus *tlr2*$^{+/+}$ zebrafish larvae under the GF condition and schematic diagram of DEGs in the representative pathways. Significantly enriched KEGG pathway terms for DEGs were determined by using the hypergeometric test/Fisher's exact test, with a threshold of *P* value < 0.05.

To validate the RNAseq findings, we performed qRT-PCR on representative DEGs for enriched pathways induced by *tlr2* deficiency under both CONVD and GF conditions. Under the CONVD condition, the qRT-PCR results were consistent with RNAseq data, confirming downregulation of *hsp70l*, *chia.3*, *hk2*, *gpib*, *pfkmb*, and *ldha*, and upregulation of *map3k5*, *gadd45ba*, *chia.2*, *amy2a*, and *kyat3* in *tlr2* mutant larvae compared to wild-type controls (Supplementary Figure 1A,B; Supplementary Table 2). Similarly, under the GF condition, the results of qRT-PCR confirmed the RNAseq data in terms of expression changes of selected representative DEGs, including upregulated *gadd45ba*, *slc3a2b* and *cel.2*, and downregulated *chia.3*, *gpib*, *grhpra*, *agxtb*, and *msmo1* in the *tlr2* mutant (Supplementary Figure 1C,D; Supplementary Table 3).

3.2. Transcriptomic responses to microbiome colonization in tlr2 mutant and wild-type larvae

To focus on the role of the microbiome in modulating host gene expression, we compared transcriptomic profiles of larvae raised under CONVD versus GF conditions within the *tlr2* mutant and wild type (Figure 2A). In wild-type larvae, a signature set of 201 DEGs was identified in the microbiome colonized group compared to the GF group (padj value < 0.05), including 17 upregulated and 184 downregulated genes (Figure 2B). In *tlr2* mutant larvae, a signature set of 127 DEGs was identified in the microbiome colonized larvae compared with the GF larvae (padj value < 0.05), including 10 upregulated genes and 117 downregulated genes (Figure 2B). Among these, only 2 upregulated and 46 downregulated DEGs were shared between *tlr2* wild-type and mutant larvae, indicating that *tlr2* strongly influences, but is not solely responsible for, the host transcriptional response to microbial colonization. This shows that only few responses to the microbiome are independent of *tlr2*. Notably, in both *tlr2* wild-type and mutant larvae, the number of downregulated DEGs consistently exceeded

the number of upregulated DEGs in CONVD larvae compared to GF larvae. Furthermore, microbiome colonization elicited a broader transcriptional response in *tlr2* wild-type larvae than in *tlr2* mutants, highlighting the essential role of *tlr2* in orchestrating host gene expression programs in response to the microbiome. Various inflammatory markers such as *atf3*, *fosl1a* and *cebpb* that were previously indicated to be downstream of TLR2 activation, are upregulated under GF conditions in the wild type (Supplementary Table 4), which is consistent with an earlier study [25].

We then performed KEGG pathway enrichment analysis on the DEGs identified under CONVD versus GF conditions within the *tlr2* mutant and wild type. The raw data for the DEGs from the representative pathways in CONVD larvae compared to GF larvae within two genotypes are shown in Supplementary table 4 and 5, respectively. In the *tlr2* wild-type larvae, enriched KEGG pathways of downregulated DEGs were dominated by metabolic pathways in general and some specific pathways. In addition, the ferroptosis pathway was enriched and all associated DEGs in this pathway were downregulated in CONVD larvae (Figure 2C). In the *tlr2* mutant larvae, enriched KEGG pathways of downregulated DEGs were no longer related to metabolism, but rather related to innate immune signaling and cellular stress responses, including Toll-like receptor signaling pathway, apoptosis and viral infection pathways. For example in apoptosis pathway, NFκB signaling-related genes including *nfkbiaa* and *nfkbiab* were downregulated in CONVD larvae (Figure 2D). These findings reveal a marked shift in the functional categories of microbiota-responsive pathways depending on *tlr2* status. Furthermore, we found that microbiome colonization led to a broad downregulation of inflammatory genes in both *tlr2* mutant and wild-type larvae (Supplementary tables 4-5). Several common inflammatory markers such as *irg1l*, *ccl20a.3*, *mmp13a_2*, *nfkbiaa*, *nos2a* and *mpeg1.2* were all downregulated in the microbiome-colonized larvae in both *tlr2* mutant and wild-type larvae. However, several downregulated genes associated with inflammation such as *mmp9*, *fosl1a*, *tnfrsf9a*, *tnfaip2b*, *timp2b*, *atf3*, and *mmp13a_1* were only downregulated in the microbiome colonized condition in the wild type.

To validate the RNAseq findings, we performed qRT-PCR on representative DEGs induced by colonized microbiome under both *tlr2* wild-type and mutant genotypes. For *tlr2* wild-type larvae, the qRT-PCR results were consistent with RNAseq data, confirming downregulation of selected genes (*acsl4b*, *tfr1b*, *fthl27*, *chia.1*, *chs1*, *cyp24a1*, *msmo1*, *cyp3c3*, *plb1*, *socs3a*

and *nfkbiaa*) in CONVD larvae compared to GF larvae (Supplementary Figure 2A,B; Supplementary Table 4). Similarly, for *tlr2* mutant larvae, qRT-PCR validation for a subset of representative genes, including *stat3*, *socs3a*, *nfkbiaa*, *gadd45ba* and *klf2a*, confirmed downregulated expression trends consistent with the RNAseq results (Supplementary Figure 2C,D; Supplementary Table 5).

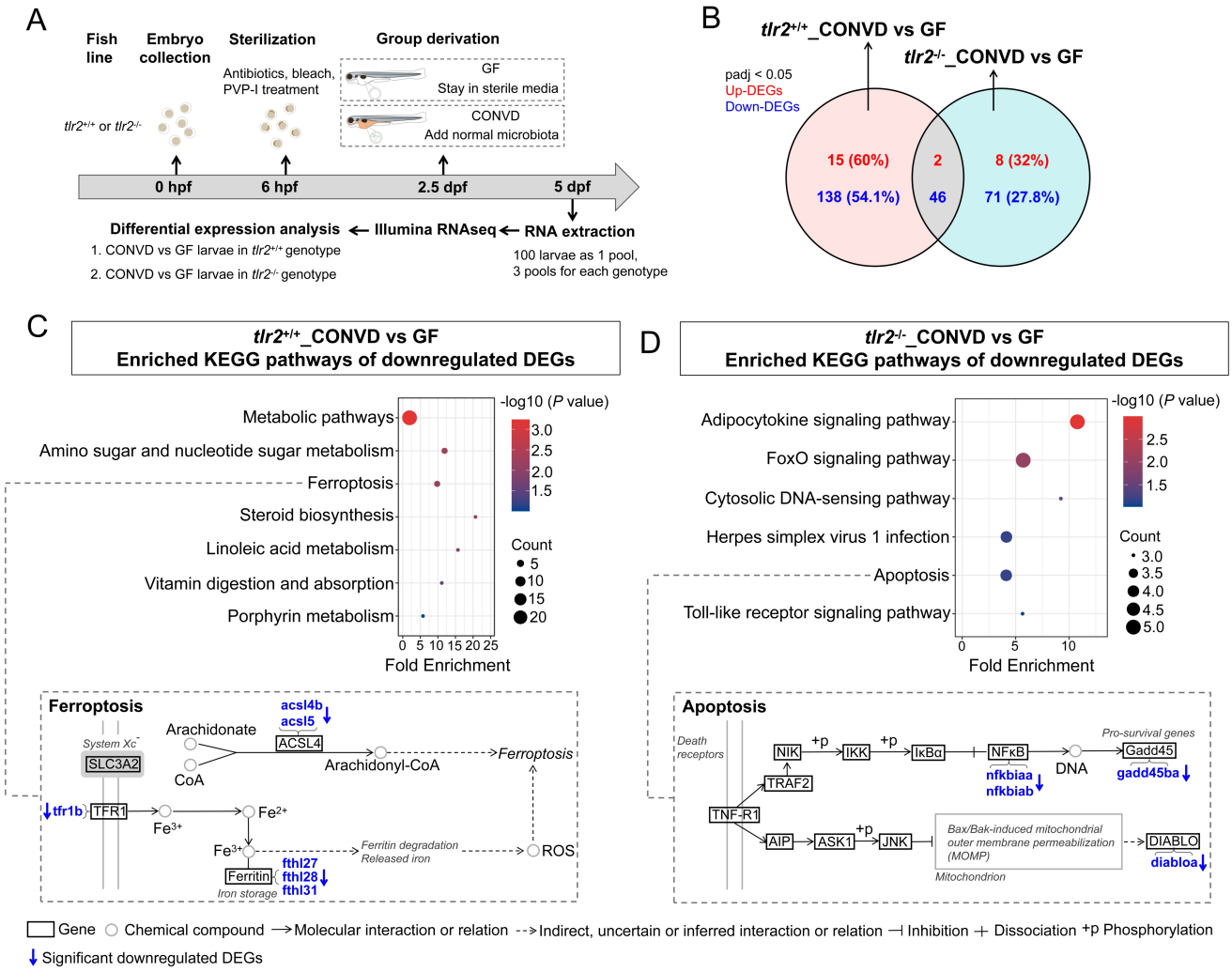

Figure 2. Differential gene expression profiles resulting from microbiome colonization in *tlr2* mutant and wild type genetic backgrounds. (A) Schematic of the experimental workflow. Conventionalized (CONVD) and germ free (GF) zebrafish larvae derived from *tlr2* wild-type and mutant lines were used to performed RNAseq at 5 days post fertilization (dpf). Differential expression analysis was conducted between CONVD and GF zebrafish larvae in *tlr2*$^{+/+}$ or *tlr2*$^{-/-}$ genetic background. (B) Numbers of upregulated and downregulated significantly differentially expressed genes (DEGs) in CONVD versus GF zebrafish larvae in *tlr2*$^{+/+}$ and *tlr2*$^{-/-}$ genetic background. DEGs were assessed by padj value less than 0.05. (C) Top 10 KEGG pathway enrichment analysis of DEGs in CONVD versus GF zebrafish larvae in *tlr2*$^{+/+}$ genotype and schematic diagram of DEGs in the representative pathways. (D) Top 10 KEGG pathway enrichment

analysis of DEGs in CONVD versus GF zebrafish larvae in *tlr2*$^{-/-}$ genotype and schematic diagram of DEGs in the representative pathways. Significantly enriched KEGG pathway terms for DEGs were determined by using the hypergeometric test/Fisher's exact test, with a threshold of P value < 0.05.

3.3. *tlr2* deficiency increases microbial diversity and alters community composition in zebrafish larvae

Considering the transcriptome alterations in various metabolic pathways in *tlr2* mutant larvae, we were interested to test whether *tlr2* mutation has an effect on the microbiome composition of the larvae compared to the wild type. Therefore, we performed 16S rRNA gene sequencing at the whole-organism level using 5 dpf *tlr2* wild-type and mutant larvae raised under conventionalized conditions (Figure 3A). The results showed that for both *tlr2* wild-type and mutant larvae, a total of 461 OTUs were identified (Supplementary Figure 3A). Principal Coordinates Analysis (PCoA) based on Bray-Curtis dissimilarity demonstrated a clear separation between *tlr2* wild-type and mutant larvae, suggesting that *tlr2* deficiency significantly alters overall microbial community structure (Figure 3B). Alpha rarefaction analysis showing plateaued curves across samples confirmed sufficient sequencing depth for reliable microbial diversity estimation (Figure 3C).

Analysis of alpha diversity indices further revealed that *tlr2* mutation markedly influenced microbial evenness, richness and diversity. Compared to wild-type controls, *tlr2* mutant larvae exhibited increased Pielou's evenness, observed species count, Shannon and Simpson diversity index (Figure 3D-G), indicating that *tlr2* deficiency leads to a more diverse and evenly distributed microbiota community during early development of zebrafish larvae.

To further understand how *tlr2* influences gut microbial composition, we analyzed taxonomic distributions of microbial communities in 5 dpf *tlr2* wild-type and mutant zebrafish larvae under conventionalized conditions at the class, family and genus levels. At the class level, Gammaproteobacteria dominated both genotypes; however, *tlr2* mutant larvae harbored significantly higher relative abundances of Bacteroidia and Alphaproteobacteria, and lower abundances of Gracilibacteria compared to wild-type controls (Supplementary Figure 4A,B). At the family level, significant differences were observed in numerous taxa. Notably, *tlr2* mutant larvae showed elevated representation of Weeksellaceae, Spirosomaceae, and Rhizobiaceae, while Gracilibacteria and Oxalobacteraceae were reduced compared to wild-type larvae (Supplementary Figure 4C,D). At the genus level, *tlr2* mutant larvae displayed

reduced levels of *Gracilibacteria* and increased abundances of genera such as *Chryseobacterium* and *Flectobacillus* (Figure 4A,B). These data demonstrate that *tlr2* is required to maintain gut microbial homeostasis not only at the level of diversity, but also in shaping the taxonomic structure of the microbiome during early zebrafish development.

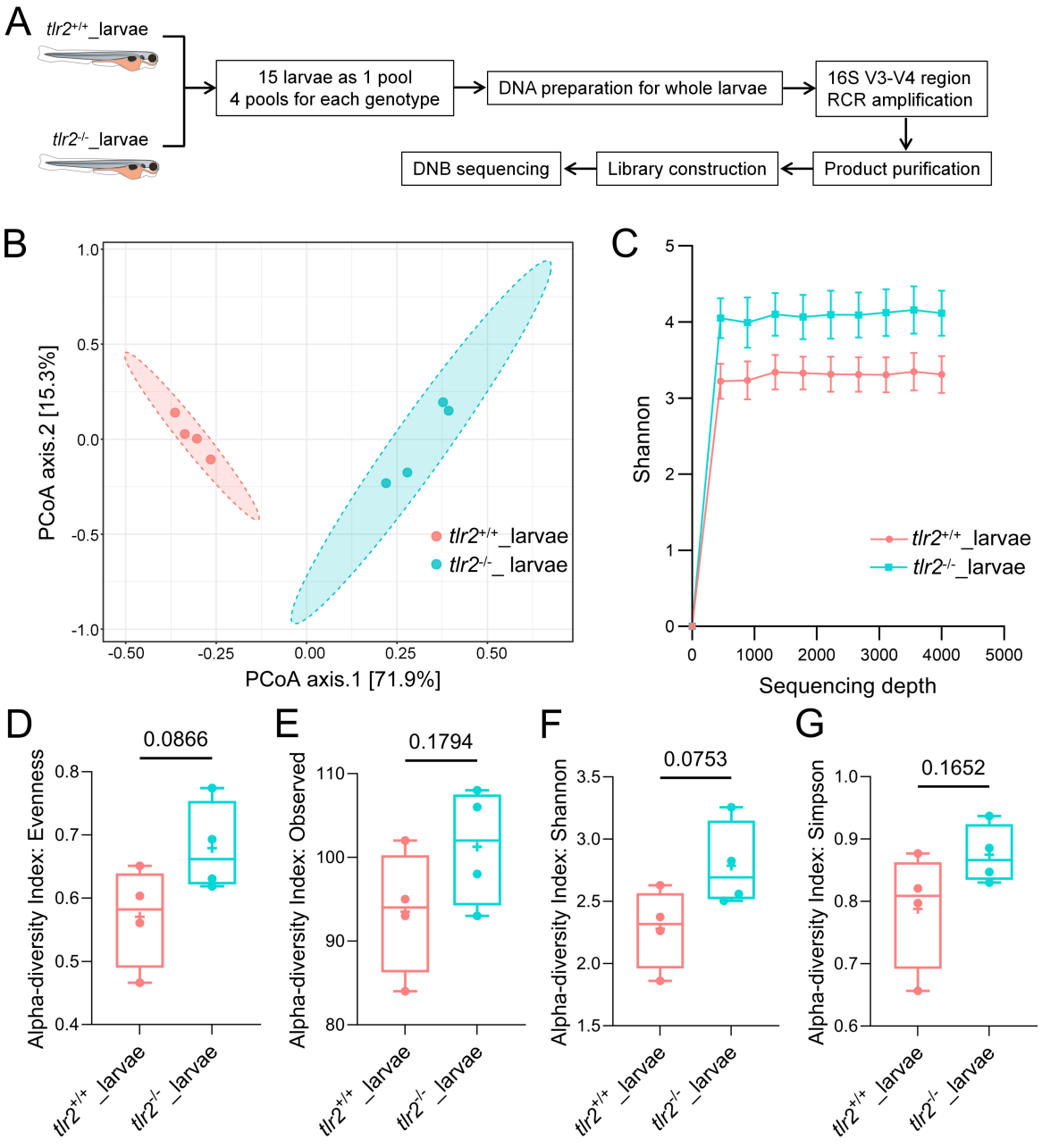

Figure 3. Overview of bioinformatics analysis of operational taxonomic units (OTUs) from *tlr2* wild type and mutant zebrafish larvae based on 16S rRNA gene sequencing. (A) Schematic of the experimental workflow. Zebrafish larvae derived from *tlr2* wild-type and mutant lines were used to performed 16S rRNA gene sequencing at 5 dpf. (B) Principal coordinate analysis (PCoA) based on Bray-Curtis distance

reveals distinct clustering of microbial communities in *tlr2*$^{+/+}$ and *tlr2*$^{-/-}$ larvae. (C) Rarefaction curves showing the observed species richness at varying sequencing depths in each genotype. (D-G) Box plots comparing alpha diversity indices, Evenness (D), Observed (E), Shannon (F) and Simpson (G) between *tlr2*$^{+/+}$ and *tlr2*$^{-/-}$ larvae. Statistical significant difference was determined by t test.

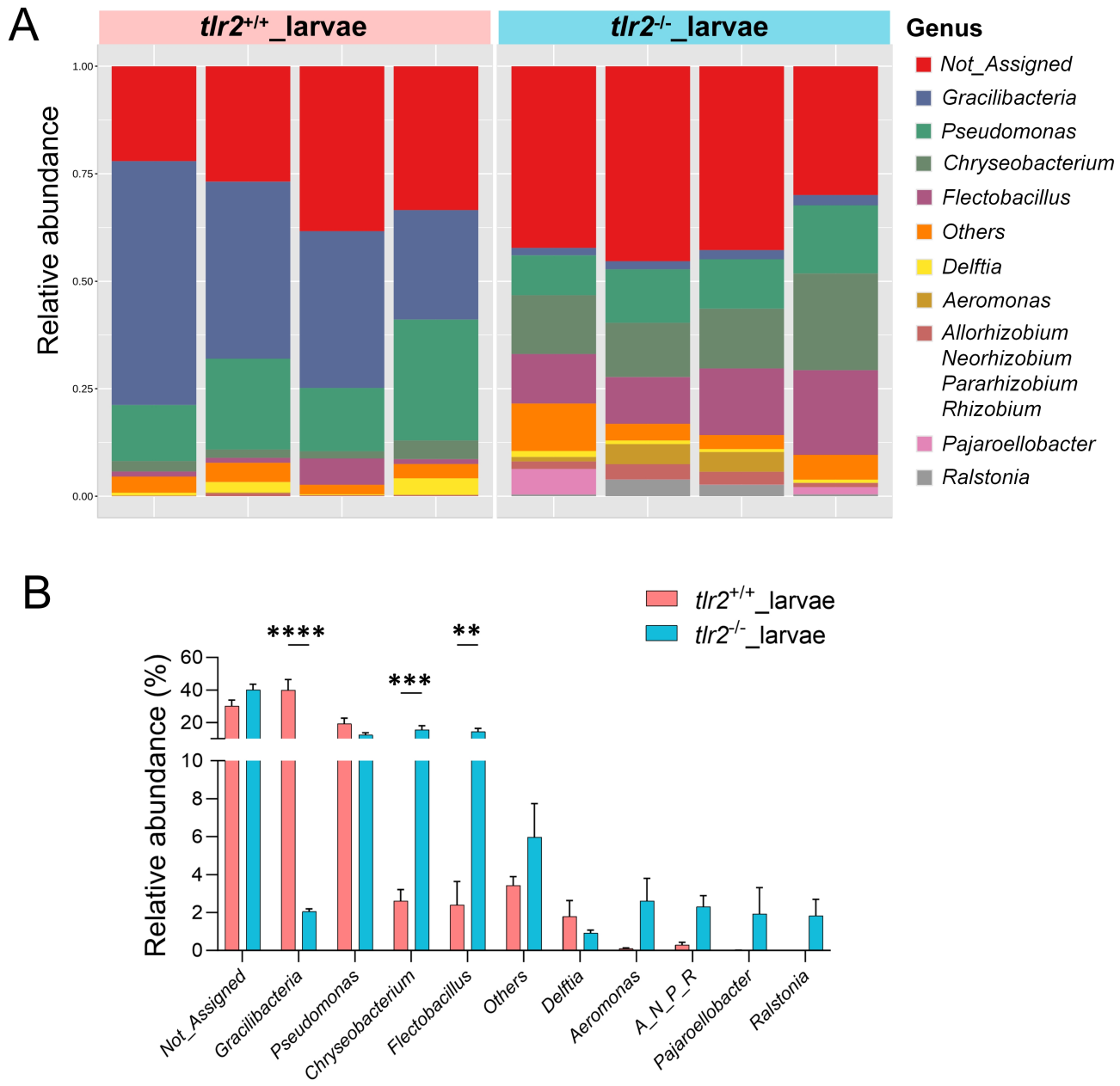

Figure 4. Composition of bacterial communities in *tlr2* wild type and mutant zebrafish larvae based on 16S rRNA gene sequencing. (A) Overview of relative abundance of the top 10 bacterial taxa at the genus level in *tlr2*$^{+/+}$ and *tlr2*$^{-/-}$ larvae. (B) Comparison of relative abundance of the top 10 bacterial taxa at the genus level between *tlr2*$^{+/+}$ and *tlr2*$^{-/-}$ larvae. The label 'Not_Assigned' refers to microbial sequences that could not be reliably classified to a known group at the taxonomic levels being displayed. The label 'Others' includes microbial groups that were present at low relative abundances and grouped together to simplify

visualization. Statistical significant difference was determined by multiple t test, **, $P < 0.01$, ***, $P < 0.001$, ****, $P < 0.0001$.

To explore the functional implications of *tlr2*-dependent microbial alterations, we performed predictive functional analysis using PICRUSt2 based on 16S rRNA gene sequencing data from zebrafish larvae. For the functional annotation analysis at MetaCyc level 2, pathways related to aldehyde degradation, glycan biosynthesis, and secondary metabolite biosynthesis were enriched in *tlr2* mutant larvae, while pathways such as pentose phosphate pathways, glycolysis and carbohydrate biosynthesis were enriched in *tlr2* wild-type larvae ($P < 0.05$, Supplementary Figure 5A). These findings indicate that *tlr2* deficiency reshapes not only the taxonomic composition but also the functional metabolic potential of the gut microbiome during early zebrafish development.

3.4. *tlr2* deficiency decreases microbial diversity and alters community composition in adult zebrafish guts

To further investigate the long-term impact of *tlr2* deficiency on gut microbial composition, we performed 16S rRNA gene sequencing on gut samples from one-year-old *tlr2* wild-type and mutant adult zebrafish (Figure 5A). The results showed that 913 OTUs were identified in *tlr2* wild-type group and 548 OTUs were identified in *tlr2* mutant group (Supplementary Figure 3B). PCoA based on Bray-Curtis dissimilarity demonstrated distinct clustering of samples according to *tlr2* genotype. Notably, *tlr2* mutant zebrafish formed separate clusters with low intra-group variation, indicating a more uniform microbial composition within this group. In contrast, *tlr2* wild type displayed broader dispersion, suggesting higher individual variability (Figure 5B). Alpha rarefaction analysis showed that all groups reached a plateau, confirming sufficient sequencing depth for diversity estimation (Figure 5C).

Analysis of alpha diversity indices revealed significant genotype-dependent differences. Specifically, *tlr2* wild-type exhibited higher microbial diversity, with significantly elevated observed species counts, Shannon diversity, Simpson index, and Pielou's evenness compared to the mutants (Figure 5D-G). These findings indicate that *tlr2* deficiency leads to restructuring of the adult gut microbiota, with a pronounced increase in diversity observed in *tlr2* wild-type guts.

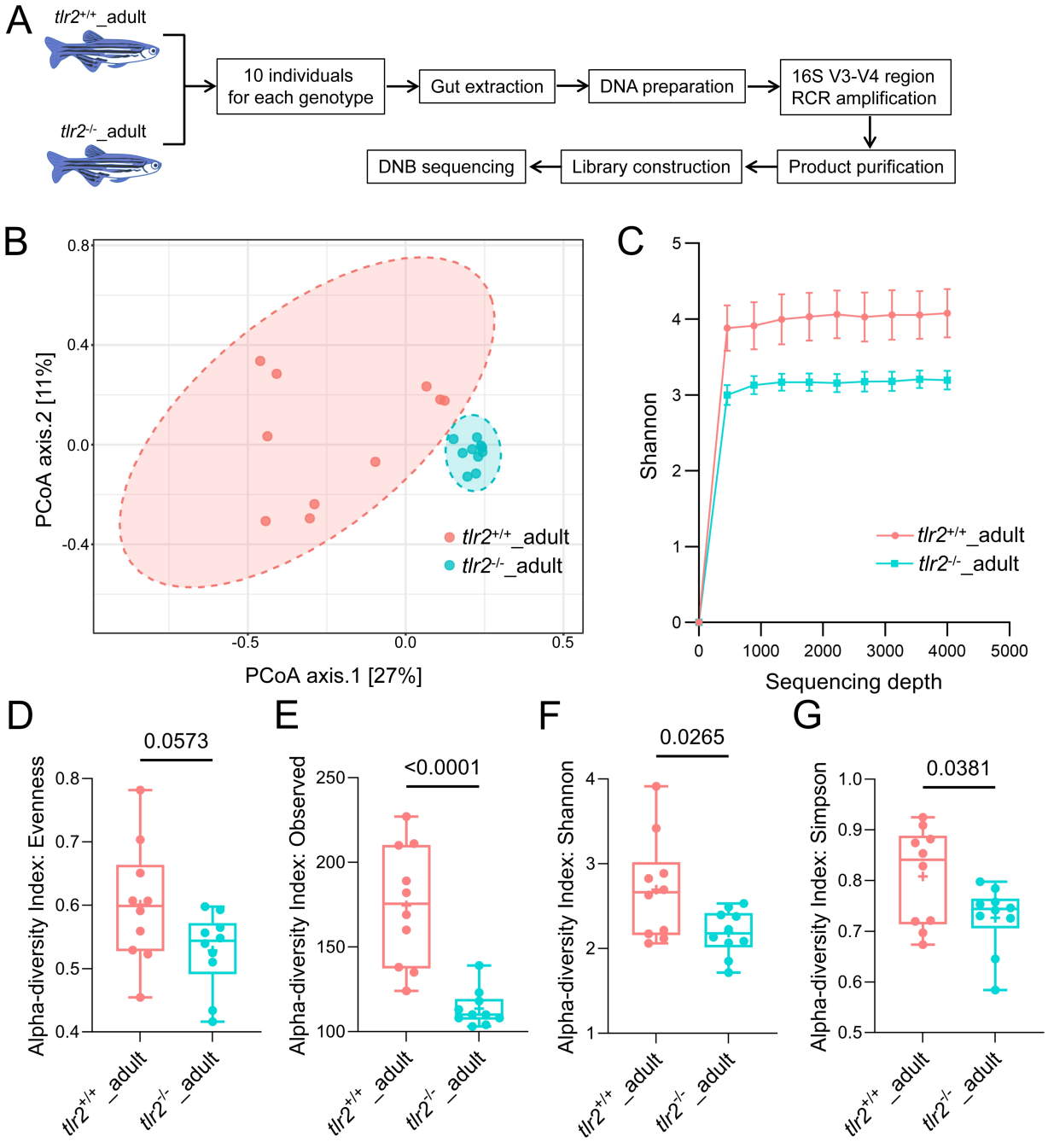

Figure 5. Overview of bioinformatics analysis of operational taxonomic units (OTUs) from *tlr2* wild type and mutant adult zebrafish guts based on 16S rRNA gene sequencing. (A) Schematic of the experimental workflow. 10 adult zebrafish derived from *tlr2* wild-type and mutant lines were performed gut extraction and the whole guts were used to performed 16S rRNA gene sequencing. (B) Principal coordinate analysis (PCoA) based on Bray-Curtis distance reveals distinct clustering of microbial communities in *tlr2*$^{+/+}$ and *tlr2*$^{-/-}$ adult guts. (C) Rarefaction curves showing the observed species richness at varying sequencing depths in each group. (D-G) Box plots comparing alpha diversity indices, Evenness (D), Observed (E), Shannon (F) and Simpson (G) between *tlr2*$^{+/+}$ and *tlr2*$^{-/-}$ adult zebrafish gut samples. Statistical significant difference was determined by t test.

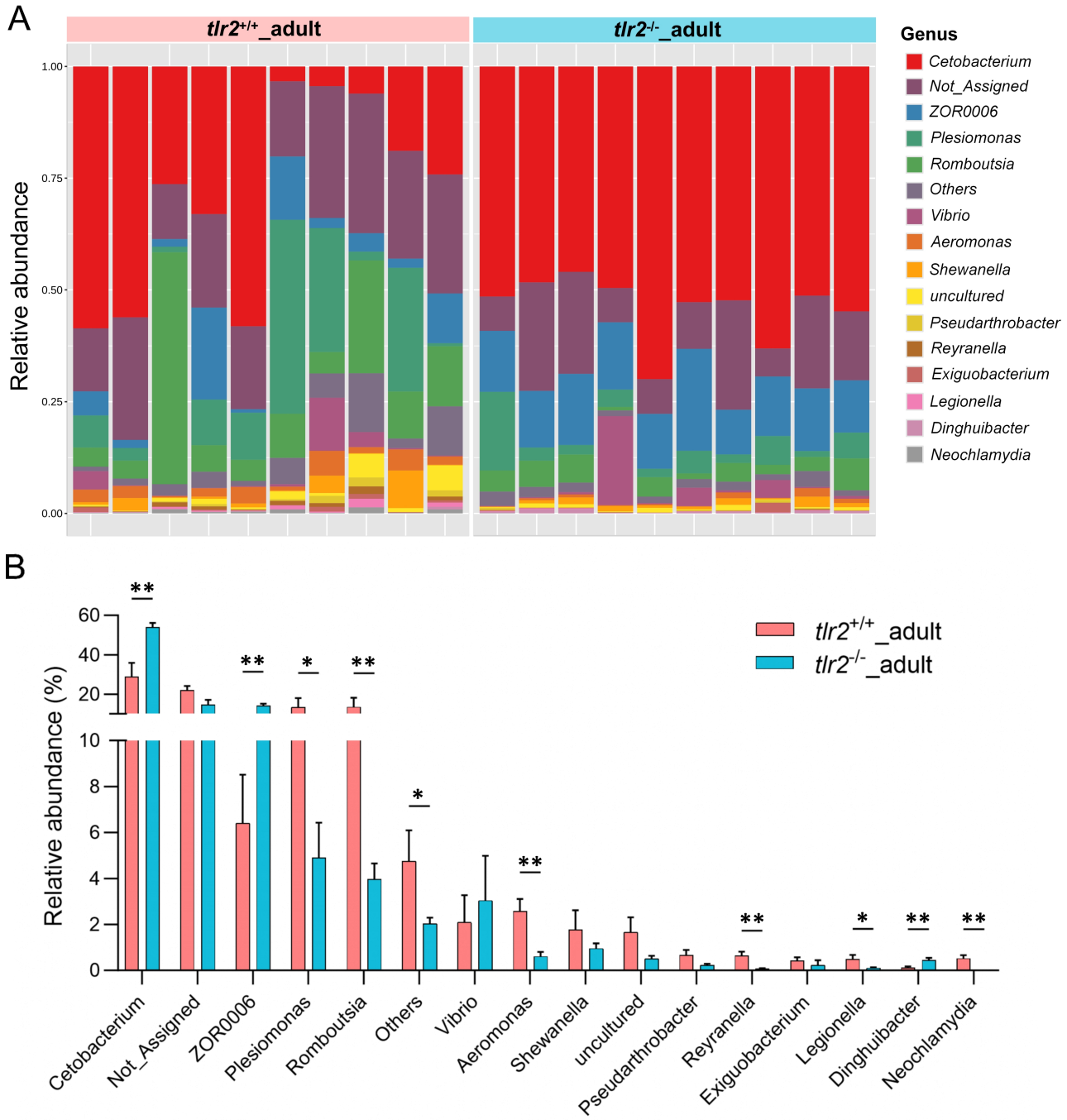

Figure 6. Composition of bacterial communities in *tlr2* wild type and mutant adult zebrafish gut based on 16S rRNA gene sequencing. (A) Overview of relative abundance of the top 15 bacterial taxa at the genus level in *tlr2*$^{+/+}$ and *tlr2*$^{-/-}$ adult zebrafish gut samples. (B) Comparison of relative abundance of the top 15 bacterial taxa at the genus level between *tlr2*$^{+/+}$ and *tlr2*$^{-/-}$ adult zebrafish gut samples. The label 'Not_Assigned' refers to microbial sequences that could not be reliably classified to a known group at the taxonomic levels being displayed. The label 'Others' includes microbial groups that were present at low relative abundances and grouped together to simplify visualization. Statistical significant difference was determined by multiple t test, *, $P < 0.05$, **, $P < 0.01$.

We also measured the taxonomic distributions of microbial communities in adult zebrafish gut samples at the genus level. Stacked bar plots and statistical comparisons revealed significant *tlr2*-dependent differences in microbial composition (Figure 6). The results show that *Cetobacterium* dominated in the *tlr2* mutant group, while *Cetobacterium* and *Plesiomonas* dominated in the *tlr2* wild-type group (Figure 6A). Genera such as *Plesiomonas*, *Romboutsia*, *Aeromonas*, *Reyranella*, *Legionella* and *Neochlamydia* were elevated in the *tlr2* wild-type group, whereas *Cetobacterium*, *ZOR0006* and *Dinghuibacter* were more abundant in the *tlr2* mutant group (Figure 6B). These results show that *tlr2* regulates gut microbial community structure in all stages from larvae to adult zebrafish, but with different consequences.

For the 16S rRNA gene sequencing data from adult zebrafish gut samples, we also conducted predictive functional profiling using PICRUSt2. MetaCyc level 2 pathway predictions showed that pathways such as chlorinated compound degradation, amine and polyamine biosynthesis, fatty acid and lipid biosynthesis, glycolysis, TCA cycle and aldehyde degradation were enriched in *tlr2* wild type. While pathways related to glycan biosynthesis, secondary metabolite biosynthesis and pentose phosphate pathways were enriched in *tlr2* mutants ($P < 0.05$, Supplementary Figure 5B).

4. Discussion

In this study, we have utilized a comparison between germ free (GF) and conventionalized (CONVD) zebrafish larvae to investigate how the microbiome influences host transcriptomic responses in a *tlr2* mutant versus wild-type control. *Vice versa*, to understand the role of Tlr2 in regulating the microbiome, we have analyzed microbial community composition in both *tlr2* mutant and wild-type zebrafish at larval and adult stages. The analysis of the composition and diversity of the microbiome by performing 16S rRNA gene sequencing allowed us to assess not only the microbial taxonomic changes as a result of *tlr2* mutation, but also to get a first insight how these microbial population changes correlate with the transcriptomic responses observed in the host.

Transcriptomic characteristics reveal TLR2-microbiome crosstalk

We compared the transcriptome profiles of *tlr2* mutant zebrafish larvae with wild-type controls first under the CONVD and then under the GF condition. Under the CONVD

condition, DEGs resulting from *tlr2* mutation were predominantly enriched in metabolic pathways, including cysteine and methionine metabolism, glycolysis/gluconeogenesis, amino sugar and nucleotide sugar metabolism. In the pathway related to glycolysis/gluconeogenesis, all associated DEGs were downregulated in the *tlr2* mutant, such as *hk2*, *gpib* and *pfkmb* (Figure 1C). This suggests that in the presence of a microbiome, *tlr2* is needed to sustain glycolytic gene expression at the whole organism level. Studies in mammalian and zebrafish models have similarly demonstrated a regulatory role of TLR2 in energy metabolism [18, 23, 32, 33]. For instance, blocking TLR2 was shown to impair mitochondrial function and suppress energy metabolism in human gastric cancer (GC) cells [32]. Infection of human dendritic cells (DCs) with *Mycobacterium tuberculosis* (Mtb) triggered HIF1A-mediated aerobic glycolysis in a TLR2-dependent manner, and this metabolic shift was essential for DC migration [33]. In unchallenged zebrafish larvae, transcriptomic and metabolomic studies showed that TLR2 has a function in glucose metabolism [18]. Notably, in this study we demonstrate that in the absence of a microbiome, *tlr2* deficiency has no effects on glycolytic metabolism, for the first time showing that *tlr2*-mediated regulation of glycolytic gene expression is microbiome-dependent. This suggests a critical interaction between TLR2 and microbiome signals in regulating host metabolic programs.

Another notable point is that under the CONVD condition, genes involved in protein processing in endoplasmic reticulum exhibited consistent downregulation in the *tlr2* mutant larvae (Figure 1C). A previous study shows that endoplasmic reticulum stress (ERS) and TLR2 expression are both upregulated in inflammatory bowel disease and ERS potentially promotes TLR2 pathway-mediated inflammatory responses [34]. However, in the *tlr2* mutant larvae this pathway was not affected under the GF condition, showing that the role of TLR2 in regulating endoplasmic reticulum stress responses is dependent on the microbiome.

Under the GF condition, *tlr2* mutant larvae displayed downregulation of ferroptosis-associated genes, including *fthl27*, *fthl28*, *fthl29*, and *fthl31*, indicating that TLR2 influences basal ferroptotic processes in the absence of microbiota (Figure 1D). This suggest a potential role for TLR2 in regulating the ferroptosis pathway due to hyperinflammation caused by the absence of microbial colonization during early larval development [25]. We also observed that in the *tlr2* mutant larvae, the presence of microbiota suppresses the apoptotic pathway, suggesting that other anti-inflammatory regulators are involved in anti-apoptotic responses to the microbiome that are distinct from ferroptosis responses as shown in Figure 2C and 2D. A

recent study has shown that TLR2 can recognize oxidized phospholipids on ferroptotic cells and facilitate downstream inflammatory responses [35]. Notably, we found that a set of ferroptosis-associated genes, including *tfr1b*, *fthl27*, *fthl28* and *fthl31* were downregulated in microbiome colonized larvae compared to the GF larvae in the wild type (Figure 2C). Recent studies have focused on gut microbiome and ferroptosis in the context of metabolic disorders, proposing them as potential therapeutic strategies for disease such as metabolic dysfunction-associated fatty liver disease (MAFLD) [36-38]. Our results demonstrate that microbial colonization modulates ferroptosis-related gene expression in a *tlr2*-dependent manner, suggesting that TLR2 may serve as a key molecular link integrating microbial signals and host ferroptotic regulation.

Analysis of canonical innate immune and inflammatory marker genes revealed that microbiome colonization led to a broad downregulation of inflammatory genes in both *tlr2* wild-type and mutant larvae (Supplementary tables 4-5). In wild-type larvae, inflammatory markers such as *atf3*, *fosl1a* and *cebpb* that were previously indicated as downstream targets of TLR2 activation, were downregulated in the microbiome-colonized larvae, which is consistent with an earlier study. Importantly, genes involved in extracellular matrix remodeling (*mmp9*, *mmp13a_1*, *timp2b*), transcription factors (*fosl1a*, *atf3*) and inflammatory signaling (*tnfrsf9a*, *tnfaip2b*) were altered only in the wild-type larvae, showing that their regulation by microbial colonization depends on functional TLR2 signaling. Furthermore, the *chia1* gene of the chitinase-like family that has been show in our earlier studies to be a reliable qRT-PCR marker of microbial inflammation was downregulated in the wild type but not in the *tlr2* mutant. In contrast, *il1b* and *socs1a* were altered only in the *tlr2* mutant larvae, suggesting that their expression may be regulated through compensatory or alternative inflammatory pathways that become engaged in the absence of TLR2.

The predominance of downregulated genes in microbiome-colonized larvae compared to germ free larvae in both genotypes possibly reflects the establishment of mucosal tolerance, a process by which intestinal immune cells and epithelia attenuate excessive responses to commensal microbes while preserving barrier integrity and immune homeostasis. As a previous study showed that zebrafish larvae exhibit strong systemic responses to microbes, future studies should aim to spatially resolve these interactions by combining tissue-specific transcriptomic approaches with in situ imaging of immune activity and single cell transcriptomic approaches.

TLR2 regulates gut microbial diversity in larval and adult zebrafish

Variations in the composition of the zebrafish gut microbiota can be influenced by both host-intrinsic and environmental factors [39, 40]. Key host-related factors include developmental stage and healthy condition. Environmental or exogenous influences such as diet composition, feeding practices (including temperature, schedule, and salinity), exposure to pathogens (including infectious microbes and viruses), antibiotic use, housing conditions, and water chemistry also play significant roles in shaping the gut microbial community [41]. In the current study, all exogenous factors were controlled by raising *tlr2* wild-type and mutant zebrafish under identical environmental conditions. Therefore, the observed differences can be attributed to host-related factors.

TLR family members are integral components of the intestinal epithelial barrier, playing critical roles in mediating the interplay between the microbiome and the immune system [42, 43]. TLR5 has been shown to regulate the composition and localization of the intestinal microbiota in mice, preventing diseases associated with low-grade inflammation and metabolic syndrome [44, 45]. Mouse Tlr2 has also been shown to influence gut microbial composition, although there was no dramatic alteration of the phylogenetic structure of microbiota in a *Tlr2* mutant, but rather an increased susceptibility to specific opportunistic bacteria [46]. In our study, *tlr2* in the zebrafish model has been shown to influence microbiome differently across life stages. In the early developmental stage at 5 days post fertilization, our results show that *tlr2* mutation changes the microbial composition and leads to increased microbial diversity (Figure 3D-G). This finding suggests that during early development, when zebrafish rely solely on innate immunity and have not yet begun feeding, *tlr2* deficiency promotes a more permissive or less selective mucosal environment, thereby facilitating the establishment of a more diverse microbiota. A previous study in the mouse model has also revealed that TLR signaling modulates mucosal selectivity and microbial colonization dynamics [15]. However, most studies in mice have focused on the adult stage. Our findings demonstrate for the first time that TLR signaling already plays a selective role in the early steps of microbial colonization with particular genera such as *Chryseobacterium* and *Flectobacillus* enriched in the mutant. These bacteria are minor constituents of adult zebrafish (Supplementary Table 6). At the larval stage, functional prediction of microbial metabolic potential indicates an under-representation of the glycolysis pathway in the *tlr2* mutant larvae (Supplementary Figure 5A). In the host transcriptome analysis, glycolysis

pathway has been shown to be suppressed in the *tlr2* mutant larvae (Figure 1C). This parallel shift in microbial metabolic potential and host gene expression highlights a bidirectional immune-metabolic crosstalk, in which *tlr2* deficiency not only reshapes microbial community function but also rewires energy metabolism of both host and microbiome. Future studies are needed to validate these associations using metabolomic approaches.

In contrast, in the adult stage when adaptive immunity is established and continued feeding for one year can contribute to individual differences, TLR2 signaling contributes to maintaining higher intestinal microbial diversity (Figure 5D-G). Dominant genera such as *Plesiomonas* and *Romboutsia*, were elevated in the *tlr2* wild type, whereas *Cetobacterium* was more abundant in the *tlr2* mutant (Figure 6B). Conversely, at the larval stage, these genera are minor constituents of the microbiome (Supplementary Table 6). These opposing results highlight the dynamic role of TLR2 in shaping microbiome composition across life stages.

The stage-dependent shifts in microbial diversity observed in *tlr2* mutants highlight the dynamic nature of host-microbiome interactions across development. While increased diversity in larvae and reduced diversity in adults may appear contradictory, such differences likely reflect distinct ecological and immunological contexts rather than opposing biological effects of *tlr2*. Moreover, given the limited taxonomic resolution of 16S rRNA gene sequencing, the functional consequences of these compositional shifts remain uncertain. Future studies using metagenomics will be required to dissect the metabolic and immunological pathways through which *tlr2* modulates microbial ecology and host responses.

Given the well-established association between pathological microbial dysbiosis, mucosal barrier dysfunction, and chronic inflammation in IBD, including Crohn's disease, our study highlights TLR2 as a potential therapeutic target [12, 16]. Modulating TLR2 signaling or leveraging TLR2-microbiota interactions may provide a novel strategy to restore mucosal immune balance and reshape the gut microbiome in IBD patients. However, for this strategy to succeed, further understanding is needed of which features within the normal microbiome are not inherently associated with the onset of pathological symptoms. Therefore, future extensive translational studies are needed to explore TLR2 or microbiome-based interventions as adjunctive therapies aimed at reestablishing intestinal homeostasis and improving disease outcomes.

5. Conclusions

In conclusion, our results demonstrate that TLR2 modulates host transcriptional responses to microbial colonization and shapes gut microbial diversity, composition, and metabolic potential. These findings underscore the critical function role of TLR2 in maintaining immune-metabolic homeostasis and provide new perspectives on its contribution to host-microbiota symbiosis throughout different developmental stages. Notably, TLR2 influences microbiome structure in a developmentally dynamic manner, as evidenced by distinct microbial profiles in larvae versus adult zebrafish. By integrating transcriptomic and microbiome analyses under germ-free and conventionalized conditions, this study establishes TLR2 as a key modulator of host-microbiome interactions and provides clues for future investigations into TLR2-targeted interventions in microbial dysbiosis-related diseases.

Supplementary Materials: Supplementary Figure 1: RNAseq data and qRT-PCR validation of representative DEGs in *tlr2*$^{-/-}$ versus *tlr2*$^{+/+}$ zebrafish larvae under CONVD and GF conditions; Supplementary Figure 2: RNAseq data and qRT-PCR validation of representative DEGs CONVD versus GF zebrafish larvae in *tlr2* wild-type and mutant genotypes; Supplementary Figure 3: Venn diagram displaying the overlap of OTUs between *tlr2*$^{+/+}$ and *tlr2*$^{-/-}$ larvae and adult gut samples; Supplementary Figure 4: Composition of bacterial communities in *tlr2* wild type and mutant zebrafish larvae based on 16S rRNA gene sequencing; Supplementary Figure 5. Differential analysis of predicted microbial functional profiles between *tlr2* wild-type and mutant zebrafish based on 16S rRNA gene sequencing; Supplementary Table 1. The primers used in this study; Supplementary Table 2. Differentially expressed genes (DEGs) in the representative pathway in *tlr2* mutant zebrafish larvae compared to the wild type controls under the CONVD condition; Supplementary Table 3. Differentially expressed genes (DEGs) in the representative pathway in *tlr2* mutant zebrafish larvae compared to the wild type controls under the GF condition; Supplementary Table 4. Differentially expressed genes (DEGs) in the representative pathway in CONVD versus GF zebrafish larvae in *tlr2* wild type background; Supplementary Table 5. Differentially expressed genes (DEGs) in the representative pathway in CONVD versus GF zebrafish larvae in *tlr2* mutant background; Supplementary Table 6. Significant genus-level microbiome differences between zebrafish larvae and adults.

Author Contributions: Initialization of study, H.P.S.; Conceptualization, H.P.S.; Sample collection, L.L.; RNAseq data analysis, L.L. and H.P.S.; 16S rRNA sequencing data analysis, L.L. and H.P.S.; Writing, L.L. and H.P.S.; Supervision, H.P.S.; All authors have read and agreed to the published version of the manuscript.

Funding: L. Liu is funded by China Scholarship Council.

Ethics approval and consent to participate: The culture of zebrafish with mutations in immune genes was approved by the local animal welfare committee (DEC) of the University of Leiden (protocol 14,198). All protocols adhered to the international guidelines specified by the EU Animal Protection Directive 2010/63/EU.

Availability of data: The raw sequencing data and analyzed expression data of RNAseq deposit in the Gene Expression Omnibus (GEO) with accession number GSE303417. The raw data of the 16S rRNA gene sequence deposit in the Sequence Read Archive (SRA) with the BioProject accession number PRJNA1291733.

Acknowledgments: We would like to thank the entire fish caretaker team at the fish facility of IBL at Leiden University for helping us take care of adult zebrafish.

Competing interests: The authors declare no competing interests.

References

[1] T. Kawai, S. Akira, The role of pattern-recognition receptors in innate immunity: update on Toll-like receptors, Nat Immunol 11(5) (2010) 373-84.
[2] Y.H. Chen, K.H. Wu, H.P. Wu, Unraveling the Complexities of Toll-like Receptors: From Molecular Mechanisms to Clinical Applications, Int J Mol Sci 25(9) (2024).
[3] L. Oliveira-Nascimento, P. Massari, L.M. Wetzler, The Role of TLR2 in Infection and Immunity, Front Immunol 3 (2012) 79.
[4] M. Correia-Neves, J. Nigou, Z. Mousavian, C. Sundling, G. Kallenius, Immunological hyporesponsiveness in tuberculosis: The role of mycobacterial glycolipids, Front Immunol 13 (2022) 1035122.
[5] X. Yu, J. Zeng, J. Xie, Navigating through the maze of TLR2 mediated signaling network for better mycobacterium infection control, Biochimie 102 (2014) 1-8.
[6] T. Kawasaki, T. Kawai, Toll-like receptor signaling pathways, Front Immunol 5 (2014) 461.
[7] D. De Nardo, Toll-like receptors: Activation, signalling and transcriptional modulation, Cytokine 74(2) (2015) 181-9.

[8] S.K. Kumar, K.P. Mani, Proinflammatory signaling mechanism of endocan in macrophages: Involvement of TLR2 mediated MAPK-NFkB pathways, Cytokine 175 (2024) 156482.
[9] Y. Mishima, A. Oka, B. Liu, J.W. Herzog, C.S. Eun, T.J. Fan, E. Bulik-Sullivan, I.M. Carroll, J.J. Hansen, L. Chen, J.E. Wilson, N.C. Fisher, J.P. Ting, T. Nochi, A. Wahl, J.V. Garcia, C.L. Karp, R.B. Sartor, Microbiota maintain colonic homeostasis by activating TLR2/MyD88/PI3K signaling in IL-10-producing regulatory B cells, J Clin Invest 129(9) (2019) 3702-3716.
[10] J.L. Round, S.M. Lee, J. Li, G. Tran, B. Jabri, T.A. Chatila, S.K. Mazmanian, The Toll-like receptor 2 pathway establishes colonization by a commensal of the human microbiota, Science 332(6032) (2011) 974-7.
[11] J.F. Burgueño, & Abreu, M. T., Epithelial Toll-like receptors and their role in gut homeostasis and disease, Nature reviews. Gastroenterology & hepatology 17 (2020) 16.
[12] L. Chen, L. Zhang, H. Hua, L. Liu, Y. Mao, R. Wang, Interactions between toll-like receptors signaling pathway and gut microbiota in host homeostasis, Immun Inflamm Dis 12(7) (2024) e1356.
[13] J.R. Marchesi, J. Ravel, The vocabulary of microbiome research: a proposal, Microbiome 3 (2015) 31.
[14] J. Lloyd-Price, G. Abu-Ali, C. Huttenhower, The healthy human microbiome, Genome Med 8(1) (2016) 51.
[15] S. Rakoff-Nahoum, J. Paglino, F. Eslami-Varzaneh, S. Edberg, R. Medzhitov, Recognition of commensal microflora by toll-like receptors is required for intestinal homeostasis, Cell 118(2) (2004) 229-41.
[16] J.L. Round, S.K. Mazmanian, The gut microbiota shapes intestinal immune responses during health and disease, Nat Rev Immunol 9(5) (2009) 313-23.
[17] T.L. Lin, Y.L. Kuo, J.H. Lai, C.C. Lu, C.T. Yuan, C.Y. Hsu, B.S. Yan, L.S. Wu, T.S. Wu, J.Y. Wang, C.J. Yu, H.C. Lai, J.C. Shu, C.C. Shu, Gut microbiota dysbiosis-related susceptibility to nontuberculous mycobacterial lung disease, Gut Microbes 16(1) (2024) 2361490.
[18] W. Hu, L. Liu, G. Forn-Cuni, Y. Ding, A. Alia, H.P. Spaink, Transcriptomic and Metabolomic Studies Reveal That Toll-like Receptor 2 Has a Role in Glucose-Related Metabolism in Unchallenged Zebrafish Larvae (Danio rerio), Biology (Basel) 12(2) (2023).
[19] J.F. Rawls, Samuel, B. S., & Gordon, J. I., Gnotobiotic zebrafish reveal evolutionarily conserved responses to the gut microbiota, Proceedings of the National Academy of Sciences of the United States of America 101 (2004) 6.

[20] S. Brugman, The zebrafish as a model to study intestinal inflammation, Dev Comp Immunol 64 (2016) 82-92.
[21] J.F. Rawls, M.A. Mahowald, R.E. Ley, J.I. Gordon, Reciprocal gut microbiota transplants from zebrafish and mice to germ-free recipients reveal host habitat selection, Cell 127(2) (2006) 423-33.
[22] C.C. Murdoch, J.F. Rawls, Commensal Microbiota Regulate Vertebrate Innate Immunity-Insights From the Zebrafish, Front Immunol 10 (2019) 2100.

[23] W. Hu, S. Yang, Y. Shimada, M. Munch, R. Marin-Juez, A.H. Meijer, H.P. Spaink, Infection and RNA-seq analysis of a zebrafish tlr2 mutant shows a broad function of this toll-like receptor in transcriptional and metabolic control and defense to Mycobacterium marinum infection, BMC Genomics 20(1) (2019) 878.
[24] L.N. Pham, M. Kanther, I. Semova, J.F. Rawls, Methods for generating and colonizing gnotobiotic zebrafish, Nat Protoc 3(12) (2008) 1862-75.
[25] B.E.V. Koch, S. Yang, G. Lamers, J. Stougaard, H.P. Spaink, Intestinal microbiome adjusts the innate immune setpoint during colonization through negative regulation of MyD88, Nat Commun 9(1) (2018) 4099.
[26] R. Patro, G. Duggal, M.I. Love, R.A. Irizarry, C. Kingsford, Salmon provides fast and bias-aware quantification of transcript expression, Nat Methods 14(4) (2017) 417-419.
[27] M.I. Love, W. Huber, S. Anders, Moderated estimation of fold change and dispersion for RNA-seq data with DESeq2, Genome Biol 15(12) (2014) 550.
[28] A. Zhu, J.G. Ibrahim, M.I. Love, Heavy-tailed prior distributions for sequence count data: removing the noise and preserving large differences, Bioinformatics 35(12) (2019) 2084-2092.
[29] K.J. Livak, T.D. Schmittgen, Analysis of relative gene expression data using real-time quantitative PCR and the 2(-Delta Delta C(T)) Method, Methods 25(4) (2001) 402-8.
[30] M. Martin, Cutadapt removes adapter sequences from high-throughput sequencing reads, EMBnet.journal 17 (2011) 3.
[31] J. Chong, P. Liu, G. Zhou, J. Xia, Using MicrobiomeAnalyst for comprehensive statistical, functional, and meta-analysis of microbiome data, Nat Protoc 15(3) (2020) 799-821.
[32] D. Cao, Y. Wu, Z. Jia, D. Zhao, Y. Zhang, T. Zhou, M. Wu, H. Zhang, T. Tsukamoto, M. Oshima, J. Jiang, X. Cao, 18beta-glycyrrhetinic acid inhibited mitochondrial energy metabolism and gastric carcinogenesis through methylation-regulated TLR2 signaling pathway, Carcinogenesis 40(2) (2019) 234-245.
[33] M. Maio, J. Barros, M. Joly, Z. Vahlas, J.L. Marin Franco, M. Genoula, S.C. Monard, M.B. Vecchione, F. Fuentes, V. Gonzalez Polo, M.F. Quiroga, M. Vermeulen, T.P. Vu Manh, R.J. Arguello, S. Inwentarz, R. Musella, L. Ciallella, P. Gonzalez Montaner, D. Palmero, G. Lugo Villarino, M.D.C. Sasiain, O. Neyrolles, C. Verollet, L. Balboa, Elevated glycolytic metabolism of monocytes limits the generation of HIF1A-driven migratory dendritic cells in tuberculosis, Elife 12 (2024).
[34] W. Wu, Y. Zhao, T. Hu, Y. Long, Y. Zeng, M. Li, S. Peng, J. Hu, Y. Shen, Endoplasmic reticulum stress is upregulated in inflammatory bowel disease and contributed TLR2 pathway-mediated inflammatory response, Immunopharmacol Immunotoxicol 46(2) (2024) 192-198.
[35] X. Luo, H.B. Gong, H.Y. Gao, Y.P. Wu, W.Y. Sun, Z.Q. Li, G. Wang, B. Liu, L. Liang, H. Kurihara, W.J. Duan, Y.F. Li, R.R. He, Oxygenated phosphatidylethanolamine navigates phagocytosis of ferroptotic cells by interacting with TLR2, Cell Death Differ 28(6) (2021) 1971-1989.
[36] J. Ji, L. Wu, J. Wei, J. Wu, C. Guo, The Gut Microbiome and Ferroptosis in MAFLD, J Clin Transl Hepatol 11(1) (2023) 174-187.

[37] G. Feng, C.D. Byrne, G. Targher, F. Wang, M.H. Zheng, Ferroptosis and metabolic dysfunction-associated fatty liver disease: Is there a link?, Liver Int 42(7) (2022) 1496-1502.
[38] A. Alisi, G. McCaughan, H. Gronbaek, Role of gut microbiota and immune cells in metabolic-associated fatty liver disease: clinical impact, Hepatol Int 18(Suppl 2) (2024) 861-872.
[39] G. Roeselers, E.K. Mittge, W.Z. Stephens, D.M. Parichy, C.M. Cavanaugh, K. Guillemin, J.F. Rawls, Evidence for a core gut microbiota in the zebrafish, ISME J 5(10) (2011) 1595-608.
[40] H.T. Yang, S.S. Zou, L.J. Zhai, Y. Wang, F.M. Zhang, L.G. An, G.W. Yang, Pathogen invasion changes the intestinal microbiota composition and induces innate immune responses in the zebrafish intestine, Fish Shellfish Immunol 71 (2017) 35-42.
[41] P. Li, J. Zhang, X. Liu, L. Gan, Y. Xie, H. Zhang, J. Si, The Function and the Affecting Factors of the Zebrafish Gut Microbiota, Front Microbiol 13 (2022) 903471.
[42] S. Frosali, D. Pagliari, G. Gambassi, R. Landolfi, F. Pandolfi, R. Cianci, How the Intricate Interaction among Toll-Like Receptors, Microbiota, and Intestinal Immunity Can Influence Gastrointestinal Pathology, J Immunol Res 2015 (2015) 489821.
[43] Y. Fang, C. Yan, Q. Zhao, B. Zhao, Y. Liao, Y. Chen, D. Wang, D. Tang, The Association Between Gut Microbiota, Toll-Like Receptors, and Colorectal Cancer, Clin Med Insights Oncol 16 (2022) 11795549221130549.
[44] M. Vijay-Kumar, Aitken, J. D., Carvalho, F. A., Cullender, T. C., Mwangi, S., Srinivasan, S., Sitaraman, S. V., Knight, R., Ley, R. E., & Gewirtz, A. T., Metabolic syndrome and altered gut microbiota in mice lacking Toll-like receptor 5, Science 328 (2010) 4.
[45] B. Chassaing, R.E. Ley, A.T. Gewirtz, Intestinal epithelial cell toll-like receptor 5 regulates the intestinal microbiota to prevent low-grade inflammation and metabolic syndrome in mice, Gastroenterology 147(6) (2014) 1363-77 e17.
[46] E.J. Albert, K. Sommerfeld, S. Gophna, J.S. Marshall, U. Gophna, The gut microbiota of toll-like receptor 2-deficient mice exhibits lineage-specific modifications, Environ Microbiol Rep 1(1) (2009) 65-70.

Supplementary Materials

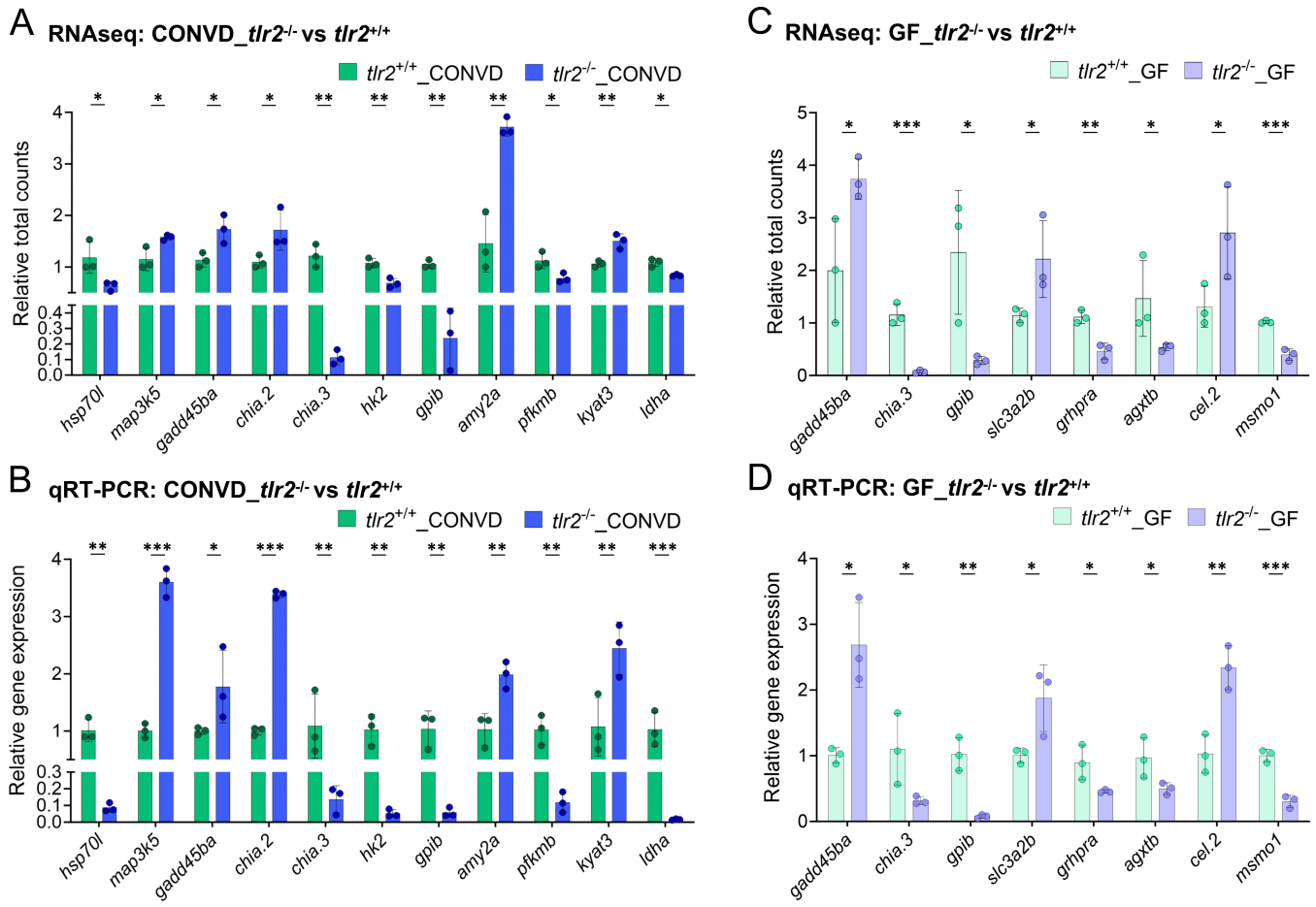

Supplementary Figure 1. RNAseq data and qRT-PCR validation of representative DEGs in *tlr2*$^{-/-}$ versus *tlr2*$^{+/+}$ zebrafish larvae under CONVD and GF conditions. (A) RNAseq results of relative expression differences of representative DEGs in *tlr2*$^{-/-}$ versus *tlr2*$^{+/+}$ zebrafish larvae under the CONVD condition. (B) qRT-PCR validation of representative DEGs in *tlr2*$^{-/-}$ versus *tlr2*$^{+/+}$ zebrafish larvae under the CONVD condition. (C) RNAseq results of relative expression differences of representative DEGs in *tlr2*$^{-/-}$ versus *tlr2*$^{+/+}$ zebrafish larvae under the GF condition. (D) qRT-PCR validation of representative DEGs in *tlr2*$^{-/-}$ versus *tlr2*$^{+/+}$ zebrafish larvae under the GF condition. Statistical significant difference was determined by multiple t test, *, P <0.05, **, P <0.01, ***, P <0.001.

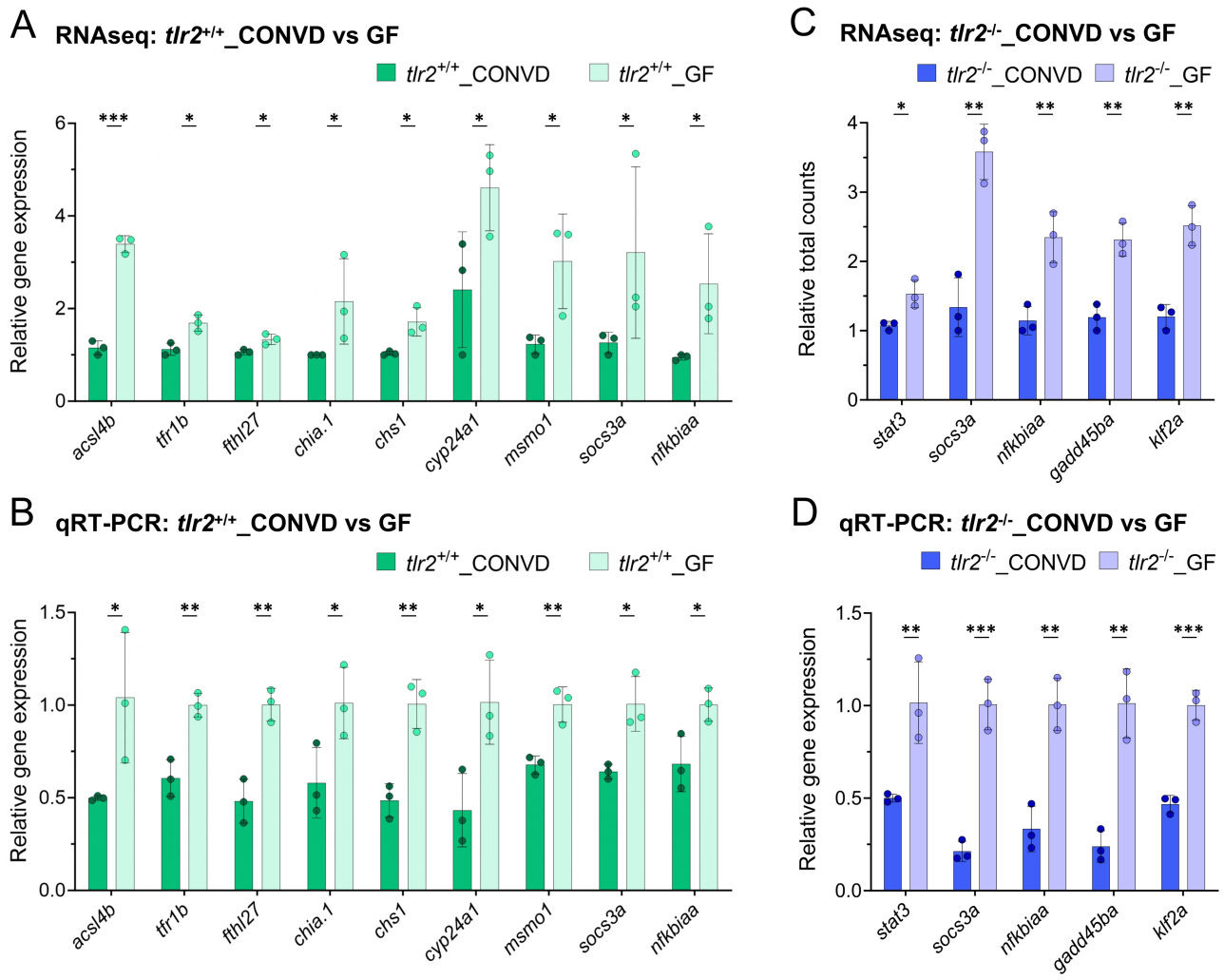

Supplementary Figure 2. RNAseq data and qRT-PCR validation of representative DEGs CONVD versus GF zebrafish larvae in *tlr2* wild-type and mutant genotypes. (A) RNAseq results of relative expression differences of representative DEGs in CONVD versus GF zebrafish larvae in *tlr2*$^{+/+}$ genotype. (B) qRT-PCR validation of representative DEGs in CONVD versus GF zebrafish larvae in *tlr2*$^{+/+}$ genotype. (C) RNAseq results of relative expression differences of representative DEGs in CONVD versus GF zebrafish larvae in *tlr2*$^{-/-}$ genotype. (D) qRT-PCR validation of representative DEGs in CONVD versus GF zebrafish larvae in *tlr2*$^{-/-}$ genotype Statistical significant difference was determined by multiple t test, *, P <0.05, **, P <0.01, ***, P <0.001.

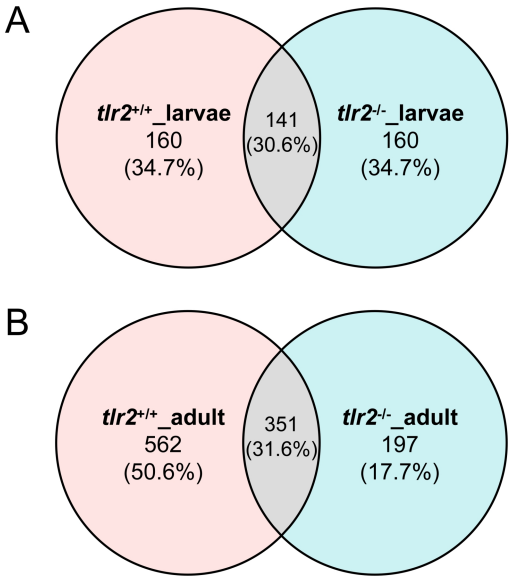

Supplementary Figure 3. Venn diagram displaying the overlap of OTUs between *tlr2*$^{+/+}$ and *tlr2*$^{-/-}$ larvae and adult gut samples. (A) The number of shared and specific OTUs of *tlr2*$^{+/+}$ and *tlr2*$^{-/-}$ larvae. (B) The number of shared and specific OTUs of *tlr2*$^{+/+}$ and *tlr2*$^{-/-}$ adult gut sample.

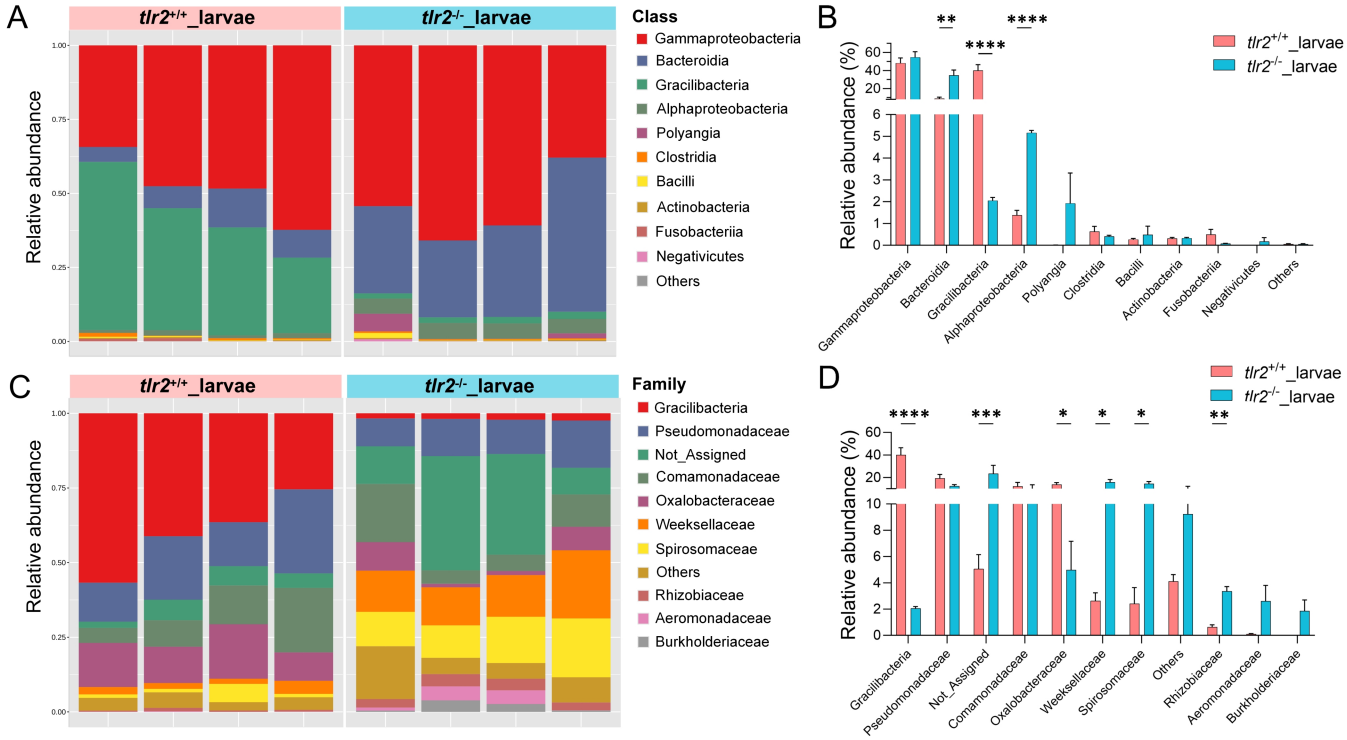

Supplementary Figure 4. Composition of bacterial communities in *tlr2* wild type and mutant zebrafish larvae based on 16S rRNA gene sequencing. Overview of relative abundance of the top 10 bacterial taxa at the class level (A) and family level (C) in *tlr2*$^{+/+}$ and *tlr2*$^{-/-}$ larvae. Comparison of relative abundance of the top 10 bacterial taxa at the class level (B) and family level (D) in *tlr2*$^{+/+}$ and *tlr2*$^{-/-}$ larvae. The

label 'Not_Assigned' refers to microbial sequences that could not be reliably classified to a known group at the taxonomic levels being displayed. The label 'Others' includes microbial groups that were present at low relative abundances and grouped together to simplify visualization. Statistical significant difference was determined by multiple t test, *, P <0.05, **, P <0.01, ***, P <0.001, ****, P <0.0001.

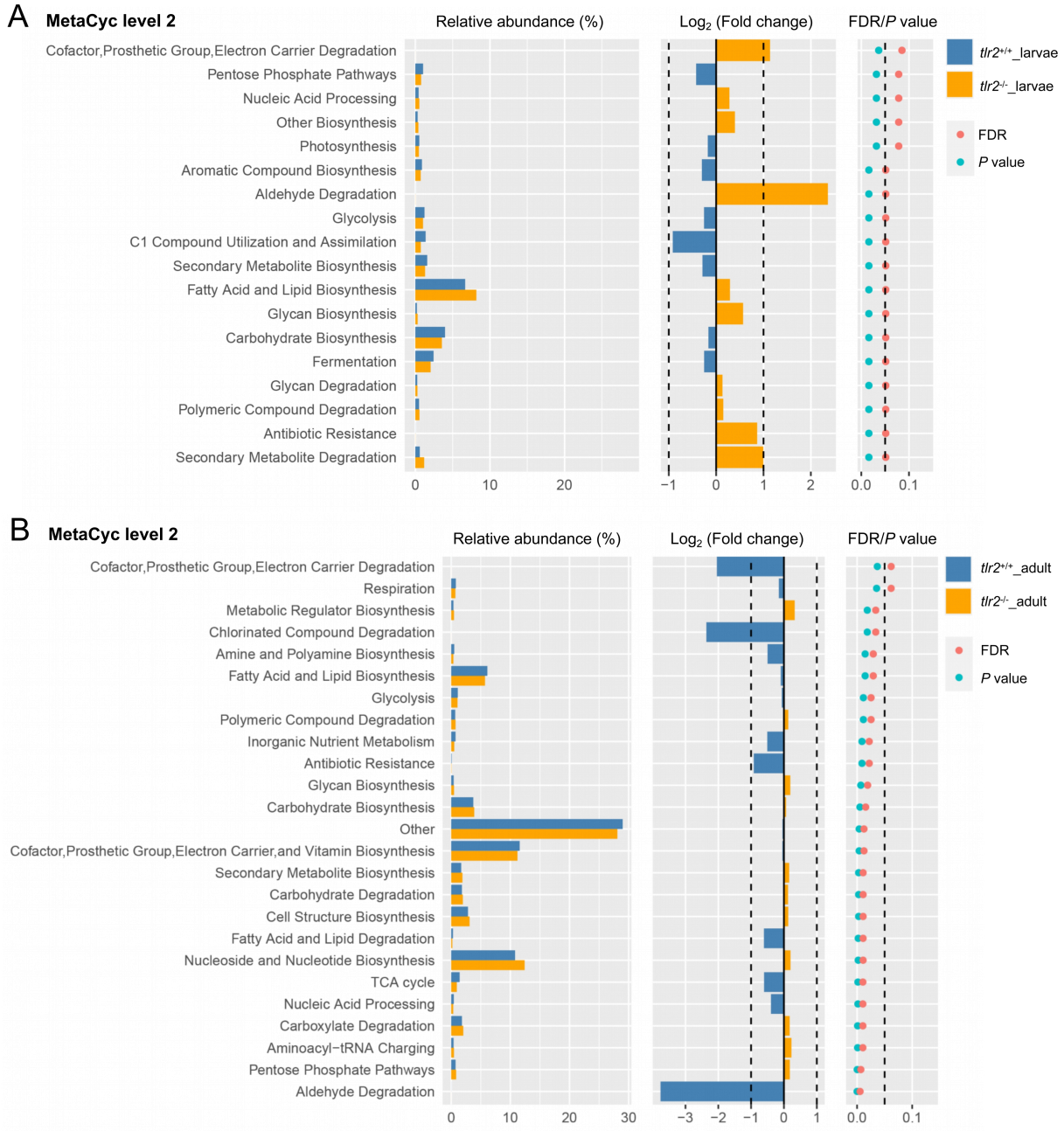

Supplementary Figure 5. Differential analysis of predicted microbial functional profiles between *tlr2* wild-type and mutant zebrafish based on 16S rRNA gene sequencing. Microbial functional profiles were predicted using PICRUSt2 based on 16S rRNA gene sequencing data. Differentially abundant level 2 MetaCyc metabolic pathways between *tlr2* wild-type and mutant zebrafish larvae (A) and adult gut samples (B) were identified using the Wilcoxon rank-sum test, with P value < 0.05 considered statistically significant.

Supplementary Table 1. The primers used in this study

Primers	Sequences	Application
hsp70l-F	5′...AGAAGTGCAATGAAGCCGTGAG...3′	qRT-PCR
hsp70l-R	5′...TCCCTGGTAGAGTTTGGAGATGAC...3′	qRT-PCR
map3k5-F	5′...AGCCTGGGAGATTTCGTGAG...3′	qRT-PCR
map3k5-R	5′...GTTGTGGTTGCGGAGGACTT...3′	qRT-PCR
ganaba-F	5′...TTATGAGACCTCTGTGGGT...3′	qRT-PCR
ganaba-R	5′...CTCCATACAGGACGAAGACC...3′	qRT-PCR
chia.1-F	5′...TGGGCATCTTGCTGTCATT...3′	qRT-PCR
chia.1-R	5′...CCAATCCTCCAACCGACAG...3′	qRT-PCR
chia.2-F	5′...CTTGGGAGCGATTCACAGG...3′	qRT-PCR
chia.2-R	5′...CGGAAAGTGCGACCGTATGT...3′	qRT-PCR
chia.3-F	5′...ATGCTGACCGCTGCTGTATC...3′	qRT-PCR
chia.3-R	5′...GTGTCCTGTGAATCGCTCCC...3′	qRT-PCR
hk2-F	5′...ACTTCAGGGTGCTCTTGGT...3′	qRT-PCR
hk2-R	5′...TGTGCCTTGCGTAATGTCTT...3′	qRT-PCR
gpib-F	5′...ATCATCGCATCCAAGACA...3′	qRT-PCR
gpib-R	5′...GTGGCAGACCATAGGGAG...3′	qRT-PCR
amy2a-F	5′...TATTTCAATGCCAACAACAAGG...3′	qRT-PCR
amy2a-R	5′...CTCTGAATCCAGCAACACCC...3′	qRT-PCR
pfkmb-F	5′...GGGACTCGCAAATGGAACTT...3′	qRT-PCR
pfkmb-F	5′...GACCAGGGCATGGATGTTAA...3′	qRT-PCR
kyat3-F	5′...ACCCAGACATTCCTCCTCCTT...3′	qRT-PCR
kyat3-R	5′...CTCATCTCCCTCCTCAACCT...3′	qRT-PCR
ldha-F	5′...TACACTTCTTGGGCTATTGG...3′	qRT-PCR
ldha-R	5′...TCTTCTGGTTTGAGGGTCAT...3′	qRT-PCR
slc3a2b-F	5′...CCCTCATTCATAACCAGACG...3′	qRT-PCR
slc3a2b-R	5′...TGACTTTAGCGAAACCCACA...3′	qRT-PCR
fthl27-F	5′...CAGATTCGCCAGAACTACGC...3′	qRT-PCR
fthl27-R	5′...ATCCAGGAAGAGCCACATCG...3′	qRT-PCR
grhpra-F	5′...GGGACTCTGATGAGCCTGTG...3′	qRT-PCR
grhpra-R	5′...ACTCGTATTCCTCGTTTCTTG...3′	qRT-PCR
agxtb-F	5′...CATCCTTGCTGAAACGGGTCT...3′	qRT-PCR
agxtb-R	5′...CAGGAATGGCAATGGTGGTG...3′	qRT-PCR
cel.2-F	5′...GGGAAAGAGTCATAGTGTTGG...3′	qRT-PCR
cel.2-R	5′...CAGGCAAGTTGTAGGAAACA...3′	qRT-PCR
msmo1-F	5′...ATGGGAGAAACAGTGGAAG...3′	qRT-PCR
msmo1-R	5′...TCGGTGGAGAAAGTAATGC...3′	qRT-PCR
acsl4b-F	5′...TGTGCTTCTGGGAGGCTGT...3′	qRT-PCR

acsl4b-R	5′...AGGCTTGTCCTGGCTGGTGT...3′	qRT-PCR
tfr1b-F	5′...TGGGTTGATGAGCACTATGT...3′	qRT-PCR
tfr1b-R	5′...TTCGTCCTGTTTCACTGTAAGC...3′	qRT-PCR
chs1-F	5′...TCGGACGCCTACACCAACT...3′	qRT-PCR
chs1-R	5′...TGGAGGGATGACAGCGATTA...3′	qRT-PCR
cyp24a1-F	5′...CGAGGCGGACGACTTTCTGT...3′	qRT-PCR
cyp24a1-R	5′...AGGCAGGCTTTGAGGTAGGG...3′	qRT-PCR
cyp3c3-F	5′...CCGATGATCCCTTTGTTAC...3′	qRT-PCR
cyp3c3-R	5′...GAATCCTTGTGCTCGTCCT...3′	qRT-PCR
plb1-F	5′...CCTACCTGGCTGGTCAAT...3′	qRT-PCR
plb1-R	5′...ACTCCCACATCCCACGCTGA...3′	qRT-PCR
socs3a-F	5′...TGACTGCGTGCTGAGACTGG...3′	qRT-PCR
socs3a-R	5′...AGATGCTGAAGCGAGGACAT...3′	qRT-PCR
nfkbiaa-F	5′...ACCTGCGTTCCATTCTTACC...3′	qRT-PCR
nfkbiaa-R	5′...CTGCTCCTTTGCGTCTACAT...3′	qRT-PCR
stat3-F	5′...GGCGTATGCGGCCAACAAG...3′	qRT-PCR
stat3-R	5′...GCCACGATGCGGGCAATCT...3′	qRT-PCR
gadd45ba-F	5′...GTCGGCGTTTATGAGTCTGC...3′	qRT-PCR
gadd45ba-R	5′...GGAGCGTGAAGTGAATCTGC...3′	qRT-PCR
klf2a-F	5′...AACAGAATAACAGACGACGAAG...3′	qRT-PCR
klf2a-R	5′...AGACGGTTGGCAGTAGGTG...3′	qRT-PCR
ppial-F	5′...TGAGCCGCAACAGTAATC...3′	Reference
ppial-R	5′...AAGGGAAAAGGAAGTGAAAG...3′	Reference
338-F	5′...ACTCCTACGGGAGGCAGCAG...3′	16S rRNA amplicon
806-R	5′...GACTACHVGGGTWTCTAAT...3′	16S rRNA amplicon

Supplementary Table 2. Differentially expressed genes (DEGs) in the representative pathway in *tlr2* mutant zebrafish larvae compared to the wild type controls under the CONVD condition

Pathway	Ensembl ID	Gene name	log2 Fold Change	FDR p-value	Description
Inflammatory markers	ENSDARG00000062788	*irg1l*	-1.966170679	7.90023E-08	immunoresponsive 1, like
	ENSDARG00000045887	*mmp30*	-1.167241743	6.85987E-10	matrix metallopeptidase 30
	ENSDARG00000101040	*ccl20a.3*	-3.876941706	0.005403424	chemokine (C-C motif) ligand 20a, duplicate 3
	ENSDARG00000013598	*tnfb*	-2.259424875	0.020288657	tumor necrosis factor b
	ENSDARG00000102175	*hamp*	-4.583273739	5.94533E-10	hepcidin antimicrobial peptide
	ENSDARG00000093303	*ifitm1*	-0.725920776	0.01617816	interferon induced transmembrane protein 1
Protein processing in endoplasmic reticulum	ENSDARG00000076888	*ganaba*	-0.370853352	0.021558697	glucosidase II alpha subunit a
	ENSDARG00000103403	*sar1b*	-0.338178978	0.033504526	secretion associated, Ras related GTPase 1B
	ENSDARG00000054807	*sec13*	-0.328320179	0.046512087	SEC13 homolog, nuclear pore

					and COPII coat complex component
	ENSDARG00000009001	*pdia6*	-0.513801914	7.13657E-05	protein disulfide isomerase family A, member 6
	ENSDARG00000021905	*derl1*	-0.419010137	0.003748342	derlin 1
	ENSDARG00000011983	*zgc:136908*	-0.522133533	0.001947588	zgc:136908
	ENSDARG00000055723	*hsp70l*	-0.918489356	0.000267796	heat shock cognate 70-kd protein, like
	ENSDARG00000092362	*hsp70.2*	-0.624316438	0.034887793	heat shock cognate 70-kd protein, tandem duplicate 2
	ENSDARG00000021924	*hsp70.3*	-1.09367763	4.60329E-07	heat shock cognate 70-kd protein, tandem duplicate 3
	ENSDARG00000010478	*hsp90aa1.1*	-1.009319213	1.7706E-06	heat shock protein 90, alpha (cytosolic), class A member 1, tandem duplicate 1
	ENSDARG00000034211	*capn2l*	-0.527630014	6.47749E-05	calpain 2, (m/II) large subunit, like
	ENSDARG00000005416	*map3k5*	0.450992698	0.001355359	mitogen-activated protein kinase kinase kinase 5
	ENSDARG00000105116	*p4hb*	-0.403907711	0.004150681	prolyl 4-hydroxylase, beta polypeptide
	ENSDARG00000015088	*dnajb11*	-0.380538578	0.011732235	DnaJ heat shock protein family (Hsp40) member B11
	ENSDARG00000041394	*dnajb1b*	-0.549618062	0.01617816	DnaJ heat shock protein family (Hsp40) member B1b
Cysteine and methionine metabolism	ENSDARG00000101791	*kyat3*	0.483299037	0.000264983	kynurenine aminotransferase 3, tandem duplicate 2
	ENSDARG00000016733	*psat1*	-0.54611994	0.000878839	phosphoserine aminotransferase 1
	ENSDARG00000101251	*ldha*	-0.388797297	0.006102055	lactate dehydrogenase A4
	ENSDARG00000054849	*bcat2*	-0.378993531	0.011145145	branched chain amino-acid transaminase 2, mitochondrial
	ENSDARG00000037706	*gss*	-0.754049556	0.023208863	glutathione synthetase
	ENSDARG00000069630	*tat*	0.672268645	0.018243442	tyrosine aminotransferase
	ENSDARG00000003132	*apip*	-1.03475855	3.61211E-09	APAF1 interacting protein
	ENSDARG00000076914	*lacc1*	-1.137693004	0.025338931	laccase (multicopper oxidoreductase) domain containing 1
Glycolysis / Gluconeogenesis	ENSDARG00000057630	*galm*	-0.673766572	0.021231597	galactose mutarotase
	ENSDARG00000101482	*hk2*	-0.656754178	0.003213	hexokinase 2
	ENSDARG00000103826	*gpib*	-2.13137979	0.000279614	glucose-6-phosphate isomerase b
	ENSDARG00000012366	*fbp2*	-0.505980784	0.034977453	fructose-1,6-bisphosphatase 2
	ENSDARG00000070826	*bpgm*	-0.469067559	0.000746983	2,3-bisphosphoglycerate mutase
	ENSDARG00000057571	*pgam2*	-0.431427662	0.001518375	phosphoglycerate mutase 2 (muscle)
	ENSDARG00000060797	*pfkmb*	-0.533927265	0.00628077	phosphofructokinase, muscle b
Amino sugar	ENSDARG00000068951	*si:ch211-*	-2.508486504	1.83189E-09	si:ch211-219a15.4

and nucleotide sugar metabolism		*219a15.4*			
	ENSDARG00000100635	*chia.1*	0.839890383	0.004368566	chitinase, acidic.1
	ENSDARG00000099185	*chia.2*	0.641380886	0.001232481	chitinase, acidic.2
	ENSDARG00000009612	*chia.3*	-3.433208212	9.41997E-40	chitinase, acidic.3
	ENSDARG00000026629	*gmds*	-0.485644245	0.035929062	GDP-mannose 4,6-dehydratase
Apoptosis	ENSDARG00000035559	*tp53*	-0.346384604	0.032871839	tumor protein p53
	ENSDARG00000003902	*ctsl.1*	0.522276485	0.00655011	cathepsin L.1
	ENSDARG00000039173	*ctslb*	4.419361688	0.038223431	cathepsin Lb
	ENSDARG00000013771	*ctss2.2*	-1.113744436	0.007652207	cathepsin S, ortholog 2, tandem duplicate 2
	ENSDARG00000044562	*cycsb*	-0.390775644	0.00600504	cytochrome c, somatic b
	ENSDARG00000058865	*endog*	-0.649397788	0.023563933	endonuclease G
	ENSDARG00000042708	*tuba8l*	-0.434601342	0.0012514	tubulin alpha 8 like
	ENSDARG00000027744	*gadd45ba*	0.597773297	0.001389775	growth arrest and DNA-damage-inducible, beta a

Supplementary Table 3. Differentially expressed genes (DEGs) in the representative pathway in *tlr2* mutant zebrafish larvae compared to the wild type controls under the GF condition

Pathway	Ensembl ID	Gene name	log2 Fold Change	FDR p-value	Description
Inflammatory markers	ENSDARG00000062788	*irg1l*	-1.232615135	0.000907275	immunoresponsive 1, like
	ENSDARG00000104795	*cxcl8a*	-1.757189375	0.037908633	chemokine (C-X-C motif) ligand 8a
	ENSDARG00000013598	*tnfb*	-1.499091857	0.029137354	tumor necrosis factor b
	ENSDARG00000045887	*mmp30*	-1.307078444	1.31495E-11	matrix metallopeptidase 30
	ENSDARG00000055278	*cfb*	-0.799539026	0.024030267	complement factor B
	ENSDARG00000087359	*c3a.2*	0.655107777	0.012800029	complement C3a, tandem duplicate 2
	ENSDARG00000060498	*tnfrsf9a*	-1.725106494	1.9046E-07	tumor necrosis factor receptor superfamily, member 9a
	ENSDARG00000026925	*nos2a*	-1.497626922	0.000506007	nitric oxide synthase 2a, inducible
	ENSDARG00000043093	*mpeg1.2*	-0.888982947	0.001797984	macrophage expressed 1, tandem duplicate 2
	ENSDARG00000102456	*cfhl4*	-0.613661133	0.029494691	complement factor H like 4
Ferroptosis	ENSDARG00000037012	*slc3a2b*	0.523041288	0.023071959	solute carrier family 3 member 2b
	ENSDARG00000037706	*gss*	-0.840177828	0.024246691	glutathione synthetase
	ENSDARG00000035559	*tp53*	-0.440378739	0.028170582	tumor protein p53
	ENSDARG00000116586	*fthl27*	-1.481742613	0.00095255	ferritin, heavy polypeptide-like 27
	ENSDARG00000076221	*fthl28*	-0.973163815	2.16539E-05	ferritin, heavy polypeptide-like 28
	ENSDARG00000113977	*fthl29*	-0.866328681	0.000208026	ferritin, heavy polypeptide-like 29
	ENSDARG00000094210	*fthl31*	-0.811793469	0.000783012	ferritin, heavy polypeptide-like

					31
Amino sugar and nucleotide sugar metabolism	ENSDARG00000068951	*si:ch211-219a15.4*	-1.667018479	8.78809E-05	si:ch211-219a15.4
	ENSDARG00000005891	*cyb5r3*	-0.51675139	0.044126112	cytochrome b5 reductase 3
	ENSDARG00000009612	*chia.3*	-4.106050627	3.55944E-83	chitinase, acidic.3
	ENSDARG00000023498	*gmppab*	-0.679146856	0.044664831	GDP-mannose pyrophosphorylase Ab
	ENSDARG00000037654	*pmm2*	-0.720361849	0.014950557	phosphomannomutase 2
	ENSDARG00000103826	*gpib*	-1.897020729	0.000572632	glucose-6-phosphate isomerase b
p53 signaling pathway	ENSDARG00000027744	*gadd45ba*	0.859081447	0.005897545	growth arrest and DNA-damage-inducible, beta a
	ENSDARG00000070272	*casp10*	-1.355160221	0.012610264	caspase 10, apoptosis-related cysteine peptidase
	ENSDARG00000044562	*cycsb*	-0.458861223	0.002982272	cytochrome c, somatic b
	ENSDARG00000078069	*rrm2*	-0.948805834	2.88862E-10	si:ch73-187m15.5
	ENSDARG00000076667	*ccng1*	-0.445389926	0.008398564	cyclin G1
Glycine, serine and threonine metabolism	ENSDARG00000068264	*grhpra*	-1.337128878	9.86622E-07	glyoxylate reductase/hydroxypyruvate reductase a
	ENSDARG00000019986	*grhprb*	-0.507411939	0.040134535	glyoxylate reductase/hydroxypyruvate reductase b
	ENSDARG00000018478	*agxtb*	-0.776032607	0.018147767	alanine--glyoxylate and serine--pyruvate aminotransferase b
	ENSDARG00000036239	*gatm*	-0.402712431	0.024246691	glycine amidinotransferase (L-arginine:glycine amidinotransferase)
Apoptosis	ENSDARG00000042708	*tuba8l*	-0.468484158	0.032233285	tubulin alpha 8 like
	ENSDARG00000013771	*ctss2.2*	-1.45194954	2.18067E-08	cathepsin S, ortholog 2, tandem duplicate 2

Supplementary Table 4. Differentially expressed genes (DEGs) in the representative pathway in CONVD versus GF zebrafish larvae in *tlr2* wild type background

Pathway	Ensembl ID	Gene name	log2 Fold Change	FDR p-value	Description
Inflammatory markers	ENSDARG00000026925	*nos2a*	-6.618517288	2.30455E-18	nitric oxide synthase 2a, inducible
	ENSDARG00000101040	*ccl20a.3*	-3.15676141	4.20257E-12	chemokine (C-C motif) ligand 20a, duplicate 3
	ENSDARG00000062788	*irg1l*	-2.606058059	1.79282E-22	immunoresponsive gene 1, like
	ENSDARG00000042816	*mmp9*	-2.443492016	0.04706782	matrix metallopeptidase 9
	ENSDARG00000015355	*fosl1a*	-1.856137931	0.002939702	FOS-like antigen 1a
	ENSDARG00000060498	*tnfrsf9a*	-1.789148838	4.66944E-06	tumor necrosis factor receptor superfamily, member 9a
	ENSDARG00000058160	*tnfaip2b*	-1.721879522	0.045066875	tumor necrosis factor, alpha-

					induced protein 2b
	ENSDARG00000043093	*mpeg1.2*	-1.020274311	0.000391775	macrophage expressed 1, tandem duplicate 2
	ENSDARG00000005481	*nfkbiaa*	-0.8445255	-0.8445255	nuclear factor of kappa light polypeptide gene enhancer in B-cells inhibitor, alpha a
	ENSDARG00000012395	*mmp13a_1*	-3.232533946	0.017492538	matrix metallopeptidase 13a
	ENSDARG00000114451	*mmp13a_2*	-5.647712699	1.46507E-06	matrix metallopeptidase 13a
	ENSDARG00000075261	*timp2b*	-2.566451995	0.004163187	TIMP metallopeptidase inhibitor 2b
	ENSDARG00000007823	*atf3*	-0.740002944	0.038490735	activating transcription factor 3
	ENSDARG00000042725	*cebpb*	-1.580266897	0.066202576	CCAAT enhancer binding protein beta
Ferroptosis	ENSDARG00000010752	*acsl4b*	-0.73056344	0.0477	acyl-CoA synthetase long chain family member 4b
	ENSDARG00000075931	*acsl5*	-0.657348787	0.004733	acyl-CoA synthetase long chain family member 5
	ENSDARG00000077372	*tfr1b*	-0.598426104	0.028813	transferrin receptor 1b
	ENSDARG00000094210	*fthl31*	-1.02391155	2.22E-08	ferritin, heavy polypeptide-like 31
	ENSDARG00000116586	*fthl27*	-1.564382897	8.92E-06	ferritin, heavy polypeptide-like 27
	ENSDARG00000076221	*fthl28*	-0.907818919	1.11E-05	ferritin, heavy polypeptide-like 28
Steroid biosynthesis	ENSDARG00000042641	*cyp51*	-0.849276369	0.018767	cytochrome P450, family 51
	ENSDARG00000055876	*msmo1*	-0.993118935	0.004445	methylsterol monooxygenase 1
	ENSDARG00000103277	*cyp24a1*	-1.574338823	0.001617	cytochrome P450, family 24, subfamily A, polypeptide 1
Amino sugar and nucleotide sugar metabolism	ENSDARG00000068515	*chs1*	-0.621183536	0.005491	chitin synthase 1
	ENSDARG00000100635	*chia.1*	-1.067004068	3.01E-06	chitinase, acidic.1
	ENSDARG00000099185	*chia.2*	-0.823021323	8.69E-06	chitinase, acidic.2
	ENSDARG00000009612	*chia.3*	-0.949796871	8.92E-05	chitinase, acidic.3
Linoleic acid metabolism	ENSDARG00000096445	*plb1*	-0.927198639	0.000574	phospholipase B1
	ENSDARG00000037873	*cyp3c3*	-0.958252459	6.94E-06	cytochrome P450, family 3, subfamily c, polypeptide 3
	ENSDARG00000103295	*cyp3a65*	-0.857568307	1.33E-06	cytochrome P450, family 3, subfamily A, polypeptide 65

Supplementary Table 5. Differentially expressed genes (DEGs) in the representative pathway in CONVD versus GF zebrafish larvae in *tlr2* mutant background

Pathway	Ensembl ID	Gene name	log2 Fold Change	FDR p-value	Description
Inflammatory markers	ENSDARG00000062788	*irg1l*	-3.337929574	1.19985E-22	immunoresponsive gene 1, like
	ENSDARG00000101040	*ccl20a.3*	-6.450217912	1.38014E-17	chemokine (C-C motif) ligand 20a, duplicate 3
	ENSDARG00000005481	*nfkbiaa*	-0.971843239	7.95028E-12	nuclear factor of kappa light polypeptide gene enhancer in B-cells inhibitor, alpha a
	ENSDARG00000043093	*mpeg1.2*	-1.26563732	7.99944E-09	macrophage expressed 1, tandem duplicate 2
	ENSDARG00000007693	*nfkbiab*	-0.455463241	0.003407582	nuclear factor of kappa light polypeptide gene enhancer in B-cells inhibitor, alpha b
	ENSDARG00000114451	*mmp13a_2*	-2.927506236	0.015367916	matrix metallopeptidase 13a
	ENSDARG00000098700	*il1b*	-2.935929644	0.024527397	interleukin 1, beta
	ENSDARG00000038095	*socs1a*	-1.148851813	2.04747E-05	suppressor of cytokine signaling 1a
	ENSDARG00000026925	*nos2a*	-3.085072068	2.23277E-06	nitric oxide synthase 2a, inducible
Adipocytokine signaling pathway	ENSDARG00000005481	*nfkbiaa*	-0.971843239	7.95028E-12	nuclear factor of kappa light polypeptide gene enhancer in B-cells inhibitor, alpha a
	ENSDARG00000007693	*nfkbiab*	-0.455463241	0.003407582	nuclear factor of kappa light polypeptide gene enhancer in B-cells inhibitor, alpha b
	ENSDARG00000025428	*socs3a*	-1.368752552	4.74737E-12	suppressor of cytokine signaling 3a
	ENSDARG00000022712	*stat3*	-0.439013991	0.049617561	signal transducer and activator of transcription 3 (acute-phase response factor)
	ENSDARG00000013721	*g6pca.2*	-0.633919405	4.7833E-07	glucose-6-phosphatase catalytic subunit 1a, tandem duplicate 2
Apoptosis	ENSDARG00000104172	*diabloa*	-0.535450977	0.000262261	diablo, IAP-binding mitochondrial protein a
	ENSDARG00000027744	*gadd45ba*	-0.896428501	2.86336E-14	growth arrest and DNA-damage-inducible, beta a
FoxO signaling pathway	ENSDARG00000025522	*sgk1*	-0.483541717	0.001128139	serum/glucocorticoid regulated kinase 1
	ENSDARG00000042667	*klf2a*	-0.993166553	2.25403E-10	Kruppel like factor 2a

Supplementary Table 6. Significant genus-level microbiome differences between zebrafish larvae and adults

	Genus	Average relative abundance (%)			
		tlr2$^{+/+}$_larvae	*tlr2*$^{-/-}$_larvae	*tlr2*$^{+/+}$_adult	*tlr2*$^{-/-}$_adult
Significant different genus in larvae	*Gracilibacteria*	39.96136	2.050383	< 0.01	0.087858312
	Chryseobacterium	2.608597	15.6802	< 0.01	< 0.01
	Flectobacillus	2.39421	14.39633	< 0.01	< 0.01
Significant different genus in adult	*Cetobacterium*	0.43122	0.072865	28.89977	53.9751
	ZOR0006	0.093925	< 0.01	6.407283	14.14808
	Plesiomonas	0.035065	0.026232	13.38108	4.908813
	Romboutsia	0.068461	0.021235	13.46754	3.974735